Stratigraphy, plankton communities, and magnetic proxies at the Jurassic/Cretaceous boundary in the Pieniny Klippen Belt (Western Carpathians, Slovakia)

JOZEF MICHALÍK[1], DANIELA REHÁKOVÁ[2], JACEK GRABOWSKI[3], OTÍLIA LINTNEROVÁ[4], ANDREA SVOBODOVÁ[5,6], JÁN SCHLÖGL[2], KATARZYNA SOBIEŃ[3] and PETR SCHNABL[6]

[1]Earth Science Institute of the Slovak Academy of Sciences, Dúbravská cesta 9, P.O. Box 106, 840 05 Bratislava, Slovakia; geolmich@savba.sk
[2]Comenius University, Faculty of Science, Dept. of Geology and Palaeontology, Ilkovičova 6, 842 15 Bratislava, Slovakia; rehakova@fns.uniba.sk; schlogl@nic.fns.uniba.sk
[3]Polish Geological Institute – National Research Institute, Rakowiecka 4, 00-975 Warsaw, Poland; jacek.grabowski@pgi.gov.pl; katarzyna.sobien@pgi.gov.pl
[4]Comenius University, Faculty of Science, Dept. of Economic Geology, Ilkovičova 6, 842 15 Bratislava, Slovakia; lintnerova@fns.uniba.sk
[5]Charles University in Prague, Faculty of Science, Institute of Geology and Palaeontology, Albertov 6, 128 43 Prague, Czech Republic; andrea.svobodova@natur.cuni.cz
[6]Czech Academy of Sciences, Institute of Geology, Rozvojová 269, 165 00 Prague 6, Czech Republic; schnabl@gli.cas.cz; asvobodova@gli.cas.cz

Abstract: A well preserved Upper Tithonian–Lower Berriasian Strapkova sequence of hemipelagic limestones improves our understanding of environmental changes occurring at the Jurassic/Cretaceous boundary in the Western Carpathians. Three dinoflagellate and four calpionellid zones have been recognized in the section. The onset of the Alpina Subzone of the standard Calpionella Zone, used as a marker of the Jurassic/Cretaceous boundary is defined by morphological change of *Calpionella alpina* tests. Calpionellids and calcified radiolarians numerically dominate in microplankton assemblages. The first occurrence of *Nannoconus wintereri* indicates the beginning of the nannofossil zone NJT 17b Subzone. The FO of *Nannoconus steinmannii minor* was documented in the lowermost part of the Alpina Subzone. This co-occurrence of calpionellid and nannoplankton events along the J/K boundary transition is typical of other Tethyan sections. Correlation of calcareous microplankton, of stable isotopes (C, O), and TOC/CaCO$_3$ data distribution was used in the characterization of the J/K boundary interval. δ^{13}C values (from +1.09 to 1.44‰ VPDB) do not show any temporal trends and thus show a relatively balanced carbon-cycle regime in sea water across the Jurassic/Cretaceous boundary. The presence of radiolarian laminites, interpreted as contourites, and relatively high levels of bioturbation in the Berriasian prove oxygenation events of bottom waters. The lower part of the Crassicolaria Zone (up to the middle part of the Intermedia Subzone) correlates with the M19r magnetozone. The M19n magnetozone includes not only the upper part of the Crassicollaria Zone and lower part of the Alpina Subzone but also the FO of *Nannoconus wintereri* and *Nannoconus steinmannii minor*. The reverse Brodno magnetosubzone (M19n1r) was identified in the uppermost part of M19n. The top of M18r and M18n magnetozones are located in the upper part of the Alpina Subzone and in the middle part of the Ferasini Subzone, respectively. The Ferasini/Elliptica subzonal boundary is located in the lowermost part of the M17r magnetozone. A little bit higher in the M17r magnetozone the FO of *Nannoconus steinmannii steinmannii* was identified.

Key words: J/K boundary, pelagic limestones, microfauna, nannoplankton, stable C and O isotopes, magnetic susceptibility, northern Tethys.

Introduction

Collection of sedimentological, geochemical and palaeontological data from complete stratigraphic sections, which can be used for correlation among candidate stratotypes of stage boundaries, is one of major goals of the Berriasian International Commission on Stratigraphy (ICS) program. A network of regional stratotypes can provide a continuous record of both sedimentation and biotic events across the Jurassic/Cretaceous boundary, and a precise evaluation of all proxies necessary for exact discrimination of the boundary position. In the Western Carpathians, the Brodno section (Michalík et al. 1990, 2009; Houša et al. 1996, 1999) represents the regional stratotype of the J/K boundary. However, ammonites are rare and sediment thickness is somewhat reduced in the Brodno

section, and complementary J/K boundary sections were thus recently studied in the Western Carpathian (Fig. 1): the Strážovce section (Borza 1984; Michalík et al. 1990); the Hlboča section (Grabowski et al. 2010) and Pośrednie sections in the Tatra Mts. (Grabowski & Pszczółkowski 2006; Grabowski et al. 2013).

Remarkable advances in calpionellid and nannoplankton biostratigraphy across the J/K boundary interval have been published on the basis of Tethyan Jurassic/Cretaceous boundary (JKB) sections (Lukeneder et al. 2010, 2015; Wimbledon et al. 2013; Svobodová & Košťák 2016). An opening of the Tethyan/Panthalassa passage between Gondwana and North America enabled phyletic evolution of small planktonic protozoans and autotrophic algae in a renewed circum-equatorial oceanic current. This evolution led to a high
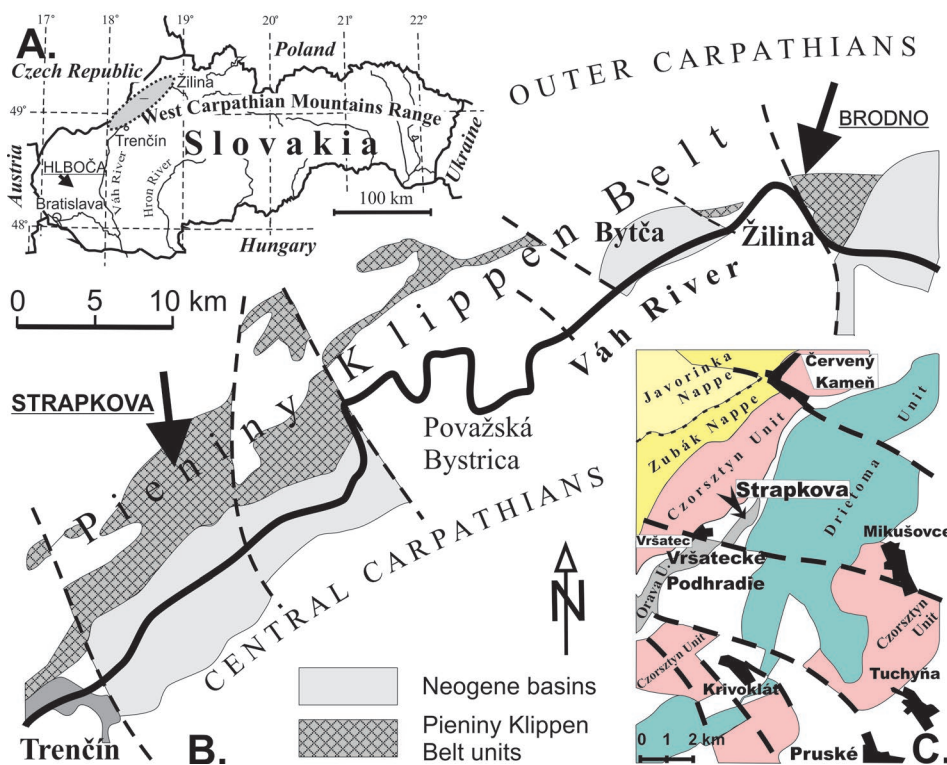
Fig. 1. A — Situation sketch of the studied area (gray ellipse) in the frame of Slovakia (arrow indicates the Hlboča section); **B** — Situation sketch of the Middle Váh Valley section of the Pieniny Klippen Belt with indication of the Brodno and Strapkova sections (arrows). **C** — Simplified geological sketch of the Pieniny Klippen Belt area between Červený Kameň, Pruské and Krivoklát villages.

regional JKB section. The distribution of the stratigraphically-important planktonic organisms revealed several coeval calpionellid and nannofossil bioevents recorded in the pelagic carbonate sequence of the JKB. The bioevents can be integrated with magnetostratigraphy. In addition, magnetic susceptibility helps us to interpret early depositional history of the sediment, namely the amount of supply of fine-grained terrigenous material to a basin.

Location of the studied sections

An important section exposing the JKB sequence in the western sector of the Pieniny Klippen Belt (Western Carpathians, Slovakia) is named the Strapkova section (Fig. 1). It can be well correlated with the principal Brodno section that is located about 40 km NE of the Strapkova section. Two additional JKB sections studied in detail (Strážovce and Hlboča) are located in the Krížna Nappe of the Central Western Carpathians (Michalík et al. 1995; Grabowski et al. 2010). The Strapkova section (49°04'09.34"N; 18°10'00.85"E; 589 m a.s.l.) is exposed on a steep SE slope of the Strapkova hill below the Mount Vršatec (Biele Karpaty Mountains, Fig. 1). It is located below a local road leading from Vršatecké Podhradie to Červený Kameň, approximately 1250 m NE from the Vršatecké Podhradie village, westwards of the middle Váh Valley. The Brodno section (49°16'02.16"N; 18°45'12.16"E; 353 m a.s.l.) has been described by Houša et al. (1996), Michalík et al. (1990, 2009) as the parastratotype section of the JKB in the Western Carpathians. It is situated in an abandoned quarry north of Žilina town on the eastern side of the narrow straits of the Kysuca River Valley (known as the "Kysuca Gate").

number of bioevents useful for global correlation of pelagic carbonate sequences. In spite of their broad spatial extent, these events differed in details due to regional palaeoenvironmental changes (Michalík & Reháková 2011). We think that the boundary level should be situated within a bundle of such events, allowing good correlations in the absence of the primary ammonite markers.

The warming in combination with eustatic oscillations could result in diverse changes of the fauna in the Panboreal Realm (Wimbledon et al. 2013; Zakharov et al. 2014). During prominent sea-level rise, connection of the Boreal sea with the Panthalassa Ocean opened as indicated by occurrences of Middle Volgian ammonites with Pacific affinity. Disturbance of the marine ecosystem indicated by green algae blooms correlates with a negative excursion of C_{org} isotope near the Volgian/Ryazanian boundary. The stratigraphic correlation is difficult between the Boreal and Tethyan bioprovinces because they underwent different evolutionary pathways, the only connecting link seems to be the magnetostratigraphy (Houša et al. 2007; Grabowski 2011; Schnabl et. al. 2015).

Our paper discusses the results of an integrated biostratigraphic study using three microplankton groups (calpionellids, calcareous dinoflagellates and nannofossils), stable isotope data ($\delta^{13}C$, $\delta^{18}O$), microfacies and sequence stratigraphy, as well as the study of magnetic record in the Strapkova section, which is regarded here as an auxiliary West Carpathian

Geological setting

The tectonic contact of two principal superunits of the Western Carpathians (the Outer and Central Carpathians) is rimmed by the Pieniny Klippen Belt (Fig. 1). This unit, originally rimming the European shelf, is typical of tensional basins-and-ridges development from the Early Jurassic until

the Palaeogene, not interrupted by Palaeoalpine tectonic movements, when the superficial nappe structure of the Central Carpathians originated. Its typical klippen-style tectonic contrasts with a slight diagenetic transformation of its rock sequences. In contrast to the Pieniny Klippen Belt, sedimentary rocks of Central Carpathian sequences are more strongly affected both by diagenesis and tectonic stress. This weak degree of diagenetic transformation thus favours a complex study of the Jurassic and Cretaceous sedimentary sections in the Pieniny Klippen Belt. They formed in two parallel shallow, but considerably subsiding marine basins separated by the Czorsztyn Ridge. The Strapkova and Brodno sections formed in more distal areas of the Kysuca Basin, in the neighbourhood of the Penninic rift system, which was gradually invaded by the Mid Atlantic-Penninic Ocean arm during the Jurassic and Cretaceous (Michalík 1994; Plašienka 2003).

Hemipelagic succession of the Strapkova section (attributed to the Orava Unit by Haško 1978 and Schlögl et al. 2000; Fig. 2) starts with the Lower Jurassic spotted limestones. An ammonite fauna indicates the Late Sinemurian Raricostatum Subzone. The Kozinec Formation composed of red pseudonodular limestones alternating with greenish-grey marly limestones contains ammonites spanning the latest Sinemurian Macdonelli Subzone of the Raricostatum Zone up to the Early Pliensbachian Davoei Zone. Grey-greenish finely bedded limestones and yellow-grey marly shales contain abundant ammonites of the Pliensbachian and Toarcian Margaritatus and Spinatum zones. Red nodular limestones following upwards are considered Toarcian in age. Well-bedded cherty spiculitic limestones of the Podzamcze Limestone Formation contain isolated beds of crinoidal packstones, capped by a 1 m thick interval of red nodular limestone (Fig. 2). The Czajakowa Radiolarite Formation is built of red radiolarites (1 m thick) with Middle Oxfordian radiolarians, a thick (1.5 m) layer of pink limestone rich in belemnite rostra and "upper" red and green radiolarites with Kimmeridgian *Saccocoma* packstones in its upper part. Radiolarites pass gradually into thin bedded red cherty and nodular limestones intercalated by red marlstones. The marlstones are followed by the Czorsztyn and the Pieniny limestone formations, which formed the subject of our study.

Methods

Microfossil and microfacies study

88 limestone beds have been sampled for thin sections. Beds have been numbered (mostly at 1 metre intervals) by numbers from 279 to 382 in accordance with former sampling (Schlögl 2001) of the entire section. The interval 301 to 324 has been omitted due to uncertainties connected with slump deformation. According to new analyses, it seems that distortion of original thickness is not significant. More densely sampled intervals (around the JKB) have been

designated according to a decimal system. Pure limestones without cherts and silicified parts were selected for thin-sections. The majority of samples have been analysed also for stable isotopes (C, O), carbonate and TOC content.

A set of 110 samples was used for microfacies analyses in order to document the succession of calpionellids and calcareous dinoflagellates. The thin-section samples were studied under the LEICA DM 2500 transmitting light microscope and the percentages of selected allochems and bioclasts (quartz and lithoclasts, calpionellids, radiolarians, globochaetes, saccocomids, filaments, clasts of benthic organisms) were calculated. The quantitative evaluation with the optical charts *sensu* Bacelle & Bosellini (1965) was used. Microfacies and biostratigraphically-important microfossils were documented using a LEICA DFC 290 HD camera. Thin-sections are stored in the collections of the Earth Science Institute of the Slovak Academy of Sciences and in the collections of the Department of Geology and Palaeontology (Faculty of Natural Sciences), both in Bratislava.

Calcareous nannofossils were analysed in 99 smear slides prepared using technique reported by Švábenická (2012) — decantation method and 7 % solution of H_2O_2. To obtain the relative sample abundances and semi-quantitative information about nannofossil species, all the specimens in at least 300 fields of view were counted in each slide. The smear slides were examined under the Olympus BX51 transmitting light microscope using an immersion objective of ×100 magnifications. Calcareous nannofossils were documented with the Olympus DP70 digital camera. The set of smear slides is stored at the Department of Geology and Palaeontology, Faculty of Science (Charles University, Prague) and at the Institute of Geology of the CAS in Prague.

Geochemistry

Stable isotopes (C, O) and total carbon (TOC) analyses were carried out on bulk rock carbonate samples. 64 samples were selected to C and O isotope analyses: 31 samples were selected in the uppermost Jurassic to the JKB interval (281–300 M) and the next 33 samples were taken in the Berriasian (325–360 M) interval. $\delta^{13}C$ and $\delta^{18}O$ were analysed in CO_2 after standard decay of bulk rock samples in 100 % phosphoric acid. Analyses of carbonate samples were done in laboratories of the Czech Geological Institute in Prague on the Finigan MAT-2 Mass Spectrometer and in the Earth Science Institute of the Slovak Academy of Sciences in Banská Bystrica on the MAT253 Mass Spectrometer equipped with the Gasbench device (Thermo Scientific Samples). Results are introduced in standard del-notation (δ) in promile (‰) being related to the Vienna Pee Bee Belemnite (VPDB) standard with 0.01 ‰ accuracy.

The palaeotemperature calculation from calcite oxygen isotopes (Anderson & Arthur 1983) is as follows: $T(°C) = 16.0 - 4.14(\delta_c - \delta_w) + 0.13(\delta_c - \delta_w)^2$, where δ_c is $\delta^{18}O$ of calcite of samples in ‰ (V-PDB) and δ_w is $\delta^{18}O$ of sea water. According to Gröcke et al. (2003), the value −1.0 ‰
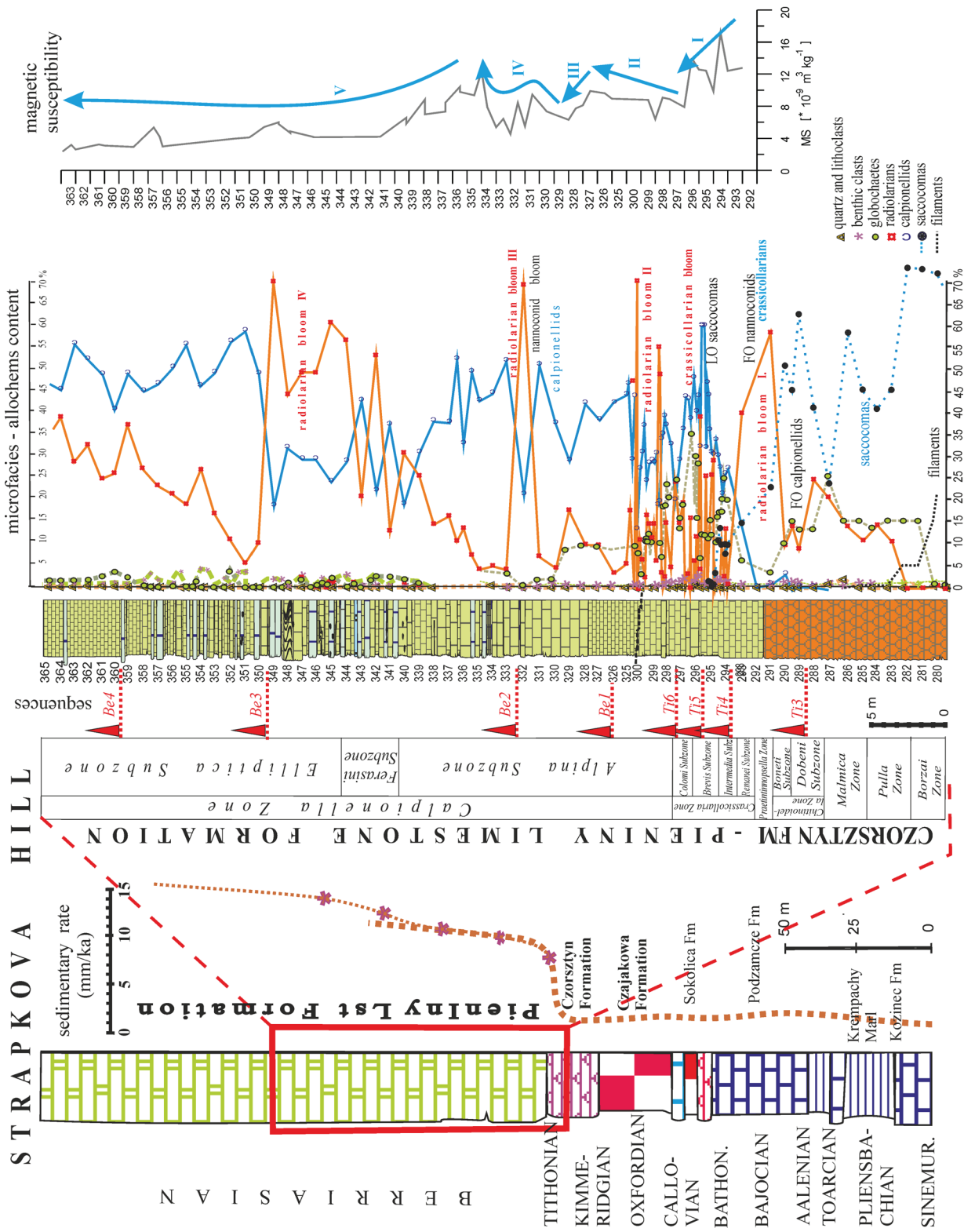
Fig. 2. Correlation of lithostratigraphy, microfacies, magnetic susceptibility of the Strapkova section sequence. **A** — general lithostratigraphy; **B** — sedimentary rate; **C** — lithological column of the sequence studied; **D** — quantitative representation of allochems in microfacies; **E** — magnetic susceptibility.

(V-SMOW) is characteristic of the post-Jurassic ice-free world. The contents of total organic carbon (TOC) and total inorganic carbon (TIC) were detected in 50 bulk rock samples on the C-MAT 5500 device of the Ströhlein Firm in the Earth Science Institute of the Slovak Academy of Sciences in Banská Bystrica. The TIC content was re-calculated on $CaCO_3$ contents.

Palaeomagnetism and magnetic properties

65 stratigraphic layers were sampled for a magnetostratigraphic study between beds 292 and 364. Samples were taken either with gasoline or electrically powered drills. Sampling resolution was usually 0.5–1 m. Standard cylindrical specimens 2.2 cm high and 2.5 cm in diameter were prepared from drill cores. Usually, at least two twin specimens were obtained from each drill core. The first specimen was subjected to thermal demagnetization and palaeomagnetic analysis, and the second one was used for rock magnetic analysis. Palaeomagnetic experiments were performed in the Palaeomagnetic Laboratories of the Polish Geological Institute-NRI in Warsaw and Institute of Geology, Czech Academy of Sciences in Prague (Průhonice). In the Palaeomagnetic Laboratory of the PGI-NRI natural remanent magnetization (NRM) was measured with the JR6a spinner magnetometer. Specimens were demagnetized exclusively by the thermal method using the MMTD1 non-magnetic oven (Magnetic Measurements, UK, rest field <10 nT). Magnetic susceptibility was monitored with a KLY-2 bridge (AGICO, Brno; sensitivity 10^{-8} SI) after each thermal demagnetization step. NRM measurements and demagnetization experiments were carried out in the magnetically shielded space (a low-field cage, Magnetic Measurements, UK, which reduces the ambient geomagnetic field by about 95 %). The thermal demagnetization was also performed in the Institute of Geology CAS using the MAVACS apparatus, the NRM was measured on the SQUID magnetometer 2G enterprises 755 4K SRM with shielded entrance. The magnetic susceptibility was measured on KLF4 magnetic susceptibility meter from AGICO. The measured data from both laboratories are fully compatible.

Results of measurements were further processed using the Remasoft software (Chadima & Hrouda 2006). Rock magnetic investigations were performed in the palaeomagnetic laboratory in Prague. They comprised mass-normalized measurements of the MS and isothermal remanent magnetization (IRM). The IRM was applied along the Z axis in the field of 1T, and then antiparallel in the field of 100mT (using MMPM10 pulse magnetizer). The S-ratio (IRM_{100mT}/IRM_{1T}) calculated as ratio of IRM intensities applied in both fields was indicative for proportions of low and high coercivity minerals. In samples from selected beds, a stepwise acquisition of the IRM (in the maximum field of 1.4T) was performed, followed by thermal demagnetization of three axes IRM acquired in the fields of 1.4T, 0.4T and 0.1T (Lowrie 1990) in order to identify magnetic minerals.

Results

Sedimentology and microfacies

The **Czorsztyn Limestone Formation** (ca. 11 m thick, samples 280 to 291, Fig. 2) is represented by red nodular limestones of the Ammonitico Rosso facies. Ammonites are affected by corrosion and dissolution and thus are very poorly preserved. The formation includes *Saccocoma*-filamentous wackestones to packstones, *Saccocoma-Globochaete*-filamentous packstones, *Saccocoma*-radiolaria-*Globochaete* packstones, *Saccocoma-Globochaete*-radiolaria packstones, *Saccocoma-Globochaete* wackestones to packstones (Fig. 3), and radiolarian wackestones. In addition to dominant bioclasts, they contain rare aptychi, crinoids (formed by twinned lamellar calcite), echinoids, juvenile ammonites, calcitic and agglutinated foraminifera, thick-walled bivalves, sponge spicules, the problematicum *Gemeridella minuta*, and calcareous dinoflagellate cysts. Dinocysts are represented by *Cadosina parvula, Colomisphaera nagyi, Stomiosphaera moluccana, Carpistomiosphaera borzai, Colomisphaera pulla, Carpistomiosphaera tithonica* (Fig. 4 A), *Colomisphaera radiata* (Fig. 4 A), *Colomisphaera carpathica* (Fig. 4 C), *Colomisphaera lapidosa, Parastomiosphaera malmica, Cadosina semiradiata fusca* (Fig. 4 D), and *Cadosina semiradiata semiradiata* (Fig. 4 E). Radiolarians and spicules are partially or totally calcified. Nodules are rimmed by dense systems of stylolites. Silt-sized muscovite flakes and quartz grains are common locally, and concentrated in the dissolution zones of stylolites. The matrix contains scattered pyrite aggregates. Saccocomas dominated in the Kimmeridgian and Lower Tithonian associations (Figs. 2, 3). Since the Late Tithonian, they were gradually replaced by *Globochaete alpina* spores.

The **Pieniny Limestone Formation** is formed by pale grey to white biomicritic limestones, with variable bed thickness. Radiolaria-*Globochaete*-calpionellids, radiolarian-calpionellid-*Globochaete*, *Globochaete-Calpionella* and calpionellid-*Globochaete*-nannofossil microfacies were identified. The abundance of bioclasts in micrite matrix varies between wackestone to packstone (Fig. 5). The limestones contain numerous calpionellids, foraminifera, *Involutina* sp. *Lenticulina* sp., benthic and planktonic crinoid segments (*Saccocoma* sp.), echinoids, ophiuroids, bivalves, juvenile ammonites, aptychi, ostracods, sponge spicules, problematicum *Didemnoides moreti*, and *Didemnum carpaticum*. Local silty quartz grains and scattered (also framboidal) pyrite occur in the matrix (Fig. 3B–F). Layers containing sedimentary breccia and synsedimentary slumps were observed locally.

Biomicrite wackestone of radiolarian-calpionellid microfacies (in 29 beds, samples from 298 to 339), contains almost the same bioclasts as those observed in the Crassicollaria Zone. Saccocomids disappeared (Fig. 5); crassicollarian loricas are currently deformed. Small bioclasts are sometimes affected by silicification; phosphatization of fragments was
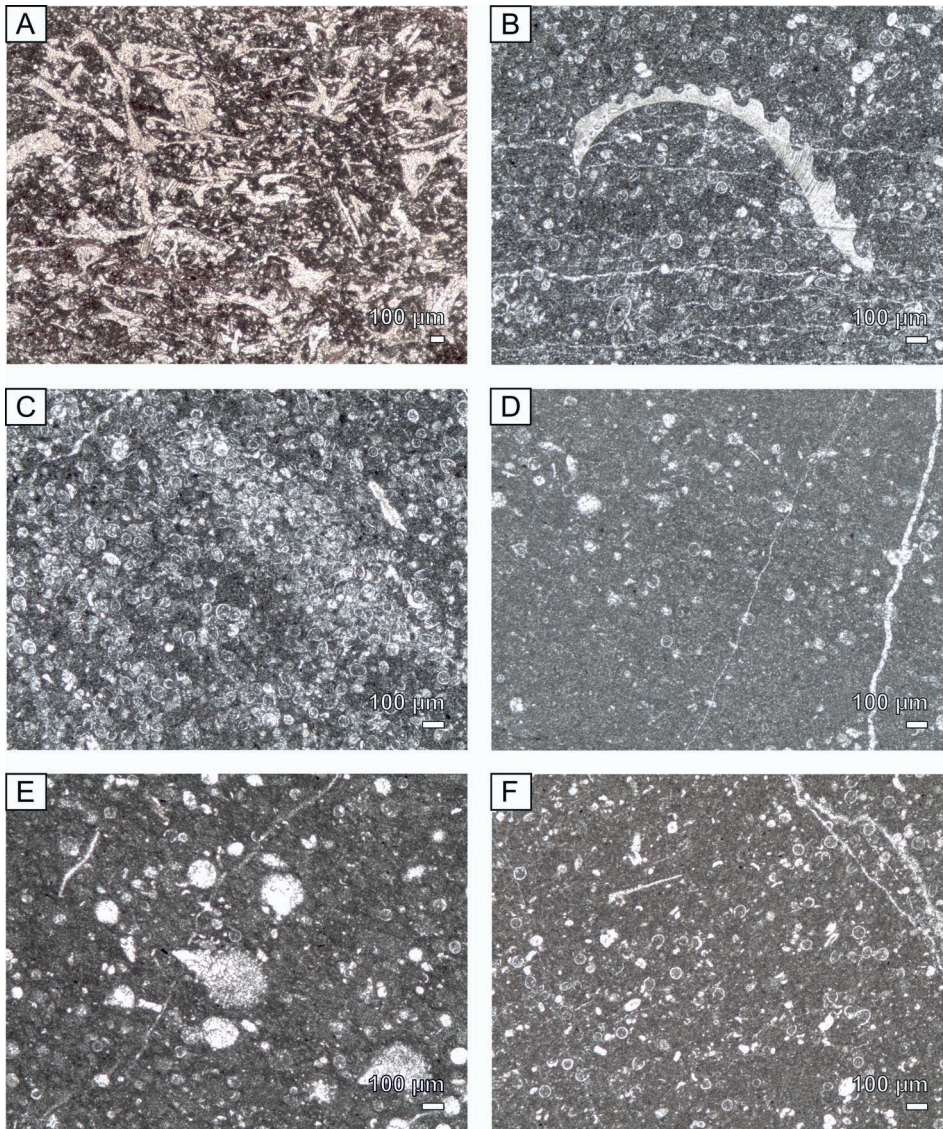
Fig. 3. Microfacies in the Strapkova section: **A** — *Saccocoma* packstone. Sample 287. **B** — Aptychi and crinoid fragments in Calpionella-*Globochaete* wackestone to packstone. Sample 296.3. **C** — Slightly bioturbated Calpionella-*Globochaete* packstone. Sample 296.3. **D** — Biomicrite radiolaria-calpionellid and Calpionella-*Globochaete* wackestone. Samples 298; 298.5. **E** — Biomicrite radiolarian wackestone. Sample 300. **F**. Biomicrite Calpionella wackestone. Sample 300.2.

Depositional environment and sequence architecture

The wackestones and packstones of the Pieniny Limestone Formation are formed mostly by tests of planktonic microorganisms, while mudstone micrites and biomicrites consist of nannoplankton remains and unidentified calcite test fragments. Although stratigraphic differences in the rock composition and in the granulometry of the "biancone" facies are not extensive, eight 7–16 m-thick cycles can be distinguished in the sequence (Fig. 2). Each of the cycle starts with packstone beds containing infrequent remnants of benthic organisms, abundant (sometimes redeposited) tests of calpionellids, occasional small (eolian) grains of quartz and mica leaflets. These beds are comparable with the lowstand part of the cycle. Upwards, limestone beds are characterized by a higher content of calcareous dinocysts and calpionellid tests. The highest part is richer in chert and frequently includes laminar concentrations of (mostly calcified) radiolarian tests. These cycles correspond to the eustatic cycles (Ti3-Ti6 and Be1-Be4) figured in Haq (2014).

The distribution of calpionellids shows several abundance peaks (Figs. 2, 5). The first peak is located in the Late Tithonian, the second peak is located in the upper part of the Alpina Subzone, and the third peak is located below the onset of the Ferasini Subzone. Stratigraphic changes in abundance of calpionellids and radiolarians (Figs. 2, 5) show that they alternate in discrete peaks: a decrease in abundance of calcareous plankton is associated with an increase of abundance of silica-secreting organisms (Reháková & Michalík 1994; Michalík et al. 2009). Locally, bioclasts are accumulated in thin laminae and small nests, some of bioclasts that are slightly phosphatized.

Radiolarians occur in very thin silicified laminae at multiple levels (I samples 315.15; 333; 339; 351.1; 381.9; 385.8; 388.25; 388.6; 393.2; 394.3; 395.15) that can be interpreted as contourites (Schlögl et al. 2000). These laminites

observed more rarely. Clastic admixture is represented by rare eolian silty quartz grains only (Fig. 2).

Silty clastic admixture content (quartz and muscovite in samples 340 to 359) is low (Fig. 2). Some layers contain laminae rich in bioclasts. Pyrite is scattered in matrix, it occurs as framboids or in nest accumulations. Several bioclasts, mainly radiolarians are impregnated by pyrite, some other bioclasts were phosphatized.

The sampling of the sequence has been complicated in the two sections in which the stratal geometry is distorted by folds (between 300–325, and 347–346). Study of sedimentology, and detailed biostratigraphy indicates that these phenomena originated synsedimentary due to rock sliding. Their presence confirms the slope environment of sedimentation.

represent a special feature of the Strapkova sequence (Fig. 6). The abundance of radiolarian tests is the highest in each fifth lamina (1.9 to 2.2 mm thick) with a slightly erosive base. Similar limestone layers with radiolarian laminae occur in the Brodno (Michalík et al. 2009; bed C42) and Rochovica sections (in the latter case, they occur in much younger, Valanginian to Aptian strata; Michalík et al. 2008).

The layer below the radiolarian laminite is bioturbated (Fig. 6A–C). Traces of *Chondrites*, *Palaeophycus*, *Planolites*, *Thalassinoides*, and *Trichichnus* were identified in cross-sections perpendicular to the bedding plane. Primary sedimentary features (cross-bedding stratification, lamination) were mostly destroyed by bioturbation. The largest burrows (*Thalassinoides*) are on average 5–9 mm in diameter, *Planolites* and *Palaeophycus* burrows attain diameters of 2 to 3 mm. *Planolites* and *Thalassinoides* burrows are penetrated by *Chondrites* (with diameters of 0.4 to 0.6 mm). Simple vertical pyritic burrows of *Trichichnus* are 0.2 mm in diameter. Framboidal pyrite clusters co-occur in places with bioturbation structures. The size of burrows, different ethological character (domichnia, fodinichnia, chemichnia) and trophic levels of these traces indicate that the bottom was well supported with nutrients and oxygen, and inhabited by burrowers at different sediment depths.
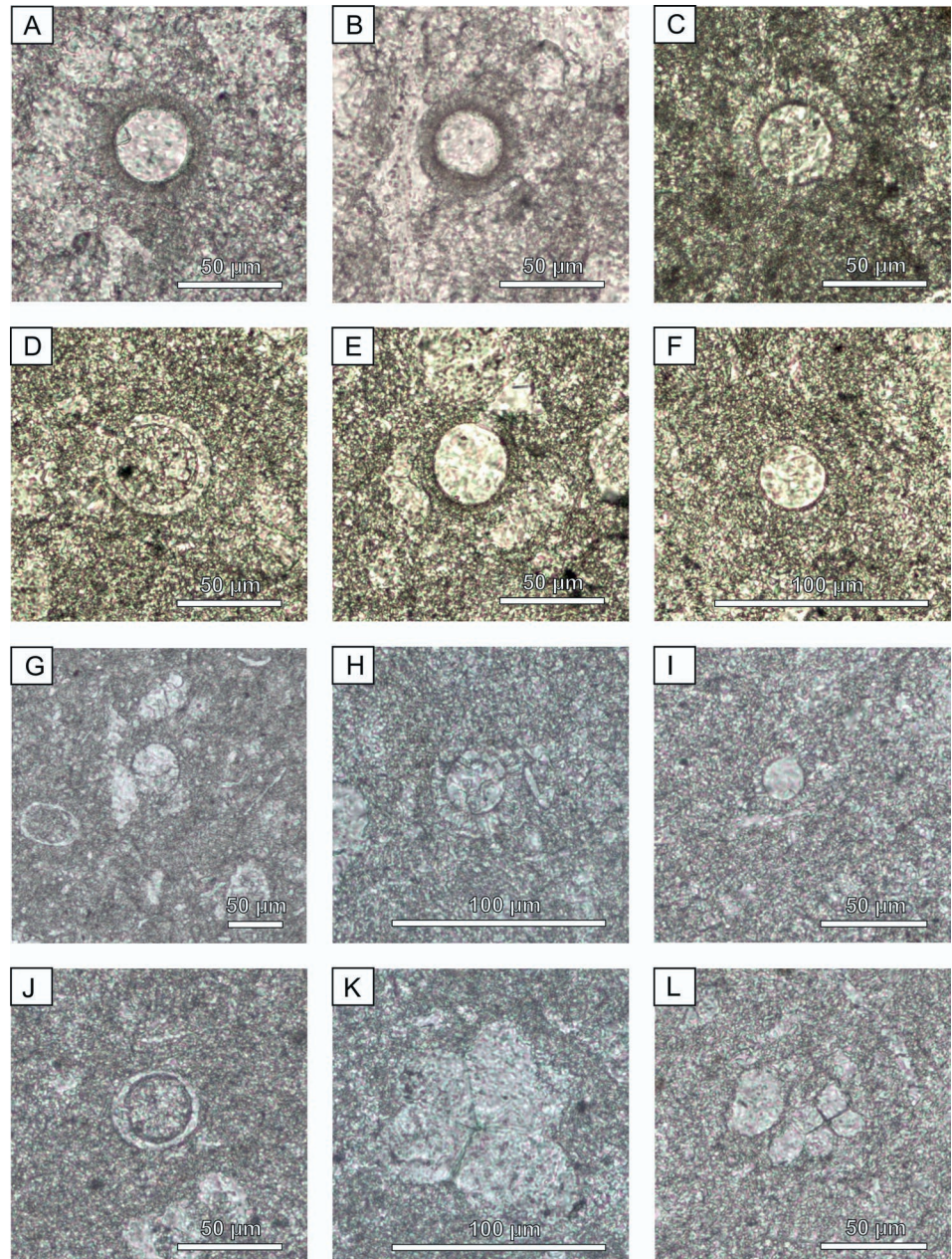

Fig. 4. Calcareous dinocysts in the Strapkova section: **A** — *Carpistomiosphaera tithonica* Nowak. Sample 287. **B** — *Colomisphaera radiata* (Vogler). Sample 287. **C** — *Colomisphaera carpathica* (Borza). Sample 287. **D** — *Cadosina semiradiata fusca* (Wanner). Sample 290. **E** — *Cadosina semiradiata semiradiata* (Wanner). Sample 290. **F, G** — *Colomisphaera fortis* Řehánek. Samples 290; 298.3. **H** — *Colomisphaera cieszynica* Nowak. Sample 300.3. **I** — *Colomisphaera lapidosa* (Colom). Sample 300.3. **J** — *Stomiosphaerina proxima* Řehánek. Sample 300.3. **K** — *Gemeridella minuta* Borza et Mišík. Sample 300. **L** — *Didemnum carpaticum* Borza et Mišík. Sample 300.1.

Biostratigraphy

Calpionellid and calcareous dinocyst zonations

Red nodular limestone of the Rosso Ammonitico facies (Czorsztyn Limestone Formation) is dated as late Kimmeridgian (Borzai and Pulla zones) to latest Early Tithonian Chitinoidella boneti Subzone (Jach et al. 2012). The succession of dinoflagellate bioevents allowed us to determine the following dinocyst zones: the Late Kimmeridgian — Borzai (sample 280) and Pulla zones (samples 281–283), and the Early Tithonian — Malmica Zone (samples 284 to 287). After a thin transitional interval (earliest Late Tithonian Praetintinopsella Zone), the sequence continues with the Maiolica facies of the Pieniny Limestone Formation (Late
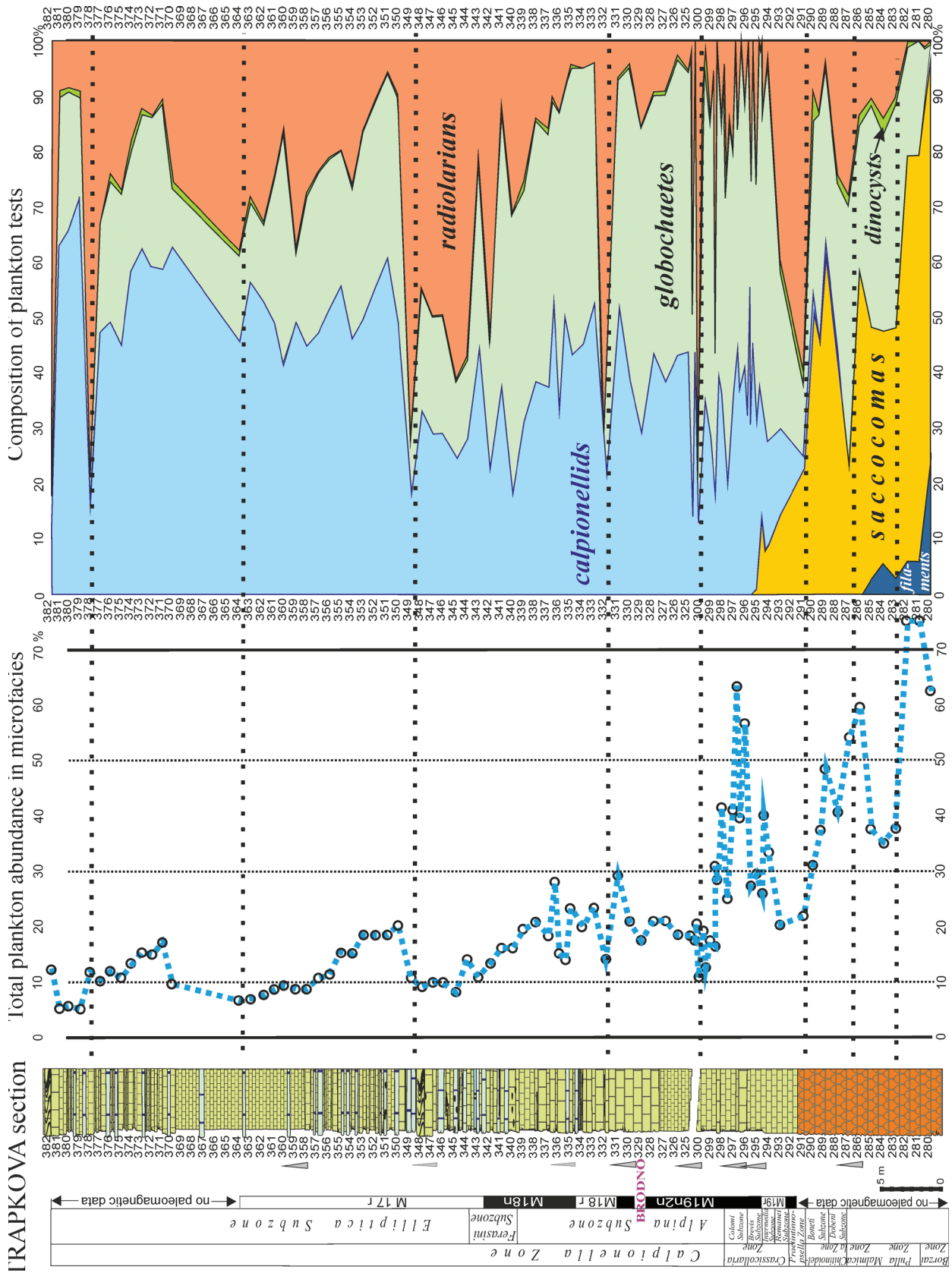
Fig. 5. Quantitative distribution of microplankton: **A** — total plankton abundance; **B** — composition of plankton groups in total plankton contents.
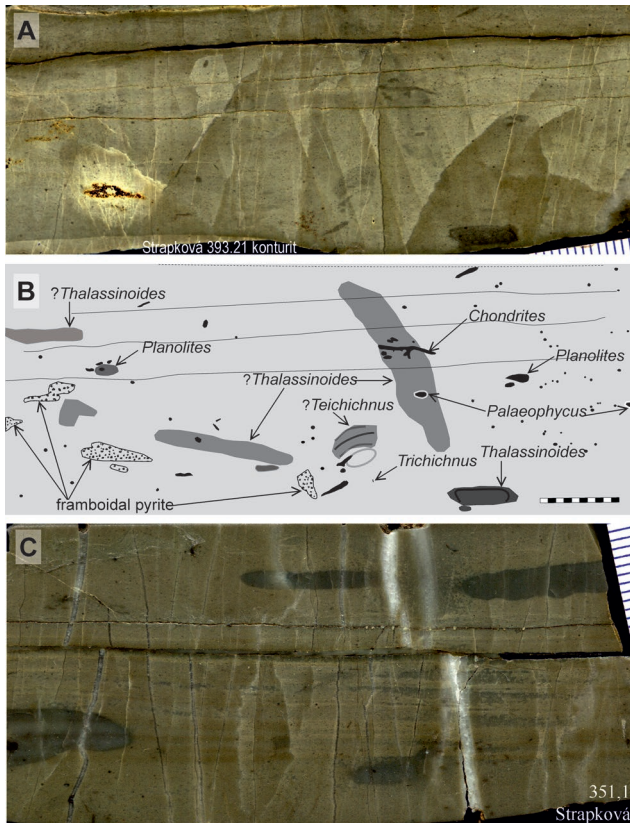
Fig. 6. Bed 393.1 of the maiolica limestone with accumulations of radiolarian tests arranged in laminae (**A**, the uppermost part). Underlying rock is penetrated by burrows of infaunal organisms (**B**) indicating more intensive oxidation (**B**) of dysoxic sediment by bottom current. **C** — Another bed (351.1) of the maiolica limestone with radiolarian tests in distinct laminae deposited from a contour current.

Tithonian to late Berriasian). Our study has been focused on the lower part of the Pieniny Formation, ca. 40 m thick (from the Late Tithonian Crassicollaria remanei Subzone to middle Berriasian Calpionella elliptica Subzone). Successive occurrence of biostratigraphically important calpionellids and calcareous dinoflagellates is shown in the Fig. 7.

Chitinoidella Zone, Dobeni Subzone
(*sensu* Grandesso 1977 and Borza 1984)

Saccocoma-Globochaete-radiolaria packstones (samples 288 to 289) contain rare *Longicollaria dobeni* (Fig. 8A) *Carpathella rumanica*, *Borziella slovenica*, *Dobeniella tithonica*, *Colomisphaera carpathica*, *Colom. lapidosa* and *Colom. tenuis*.

Chitinoidella Zone, Boneti Subzone
(*sensu* Grandesso 1977 and Borza 1984)

Saccocoma-Globochaete-radiolaria packstones and *Saccocoma-Globochaete* wackestones to packstones (samples 289.4–290) with *Chitinoidella boneti* (Fig. 8B), *Chitin. elongata* (Fig. 8C), *Longicollaria dobeni*, *Dobeniella cubensis*, *Popiella oblongata*, *Colomisphaera carpathica*, *Colom. lapidosa*, *Colom. tenuis* and *Colom. fortis* (Fig. 4F, G).

Praetintinnopsella Zone (*sensu* Grandesso 1977)

Radiolaria wackestones (sample 291) contain rare chitinoidellids, cysts of *Colomisphaera carpathica* but also the first hyaline calpionellid form represented by *Praetintinnopsella andrusovi* (Fig. 8E).

Crassicollaria Zone, Remanei Subzone
(*sensu* Remane et al. 1986)

Radiolarian wackestone (sample 293) with very rare sections of microgranular chtitinoidellids contains *Tintinopsella remanei* (Fig. 8D), *Calpionella alpina, Crassicollaria intermedia,* and cysts of *Colomisphaera carpathica*.

Crassicollaria Zone, Intermedia Subzone
(*sensu* Remane et al. 1986)

Calpionella-*Globochaete* locally slightly laminated wackestones to packstones (8 beds from 294 to 294.6) with *Crassicollaria intermedia* (Fig. 8F), *Crass. parvula*, *Crass. massutiniana* (Fig. 8G), *Calpionella alpina*, *Calp. grandalpina* (Fig. 8K), *Calp. elliptalpina*, *Tintinnopsella carpathica,* and cysts of *Colomisphaera lapidosa, Colom. carpathica*, *Stomiosphaerina proxima*, *Cadosina semiradiata semiradiata,* and *Cadosina* sp.

Crassicollaria Zone, Brevis Subzone
(*sensu* Reháková & Michalík 1997)

Radiolarian-Calpionella-*Globochaete*, Calpionella-*Globochaete*, *Globochaete*-Calpionella, locally slightly laminated and/or bioturbated wackestones (18 beds from 294.7 to 296.2) contain *Crassicollaria brevis* (Fig. 8H), *Crassicollaria parvula*, *Calpionella alpina*; *Crassicollaria massutiniana*, *Calpionella grandalpina*, *Tintinnopsella carpathica*, cysts of *Colomisphaera lapidosa*, *Colomisphaera carpathica*, *Stomiosphaerina proxima*, *Cadosina semiradiata semiradiata* and *Cadosina semiradiata fusca* are less abundant if compared with the Intermedia Subzone.

Crassicollaria Zone, Colomi Subzone
(*sensu* Reháková & Michalík 1997)

The FO of *Crassicollaria colomi* was identified in slightly bioturbated biomicrite (16 beds from 296.3 to 297) with Calpionella-*Globochaete* (Fig. 3B, C), radiolarian-Calpionella, radiolarian-Calpionella-*Globochaete* and radiolarian microfacies. *Crassicollaria parvula* dominates over *Crass. colomi* (Fig. 8I), *Crass. brevis*, *Crass. massutiniana,* and *Calpionella alpina* (Fig. 8J), which prevails over *Calpionella grandalpina* and *Tintinnopsella carpathica*. *Colomisphaera lapidosa, Colom. carpathica*, *Stomiosphaerina proxima*, *Cadosina semiradiata semiradiata*, *Cados. semiradiata fusca* cysts were also identified.

Calpionella Zone, Alpina Subzone
(*sensu* Pop 1974; Remane et al. 1986;
Reháková & Michalík 1997; Lakova et al.1999;
Boughdiri et al. 2006; Andreini et al. 2007;
Lakova & Petrova 2013).

Biomicrite wackestone is composed of radiolarian, radiolarian-calpionellid and calpionellid microfacies (29 beds between 298–339; Fig. 3E, F). The sample 298 shows transition from the microfacies rich in *Crassicollaria parvula* to microfacies in which spherical forms of *Calpionella alpina* dominate. Thus, the J/K boundary interval according to Remane's et al. (1986) definition is situated in bed 298. Four crassicollarian abundance events influenced by synsedimentary erosion were documented (samples 298.1–298.4). Since the sample 298.6, Calpionella-*Globochaete* wackestones prevail (Fig. 3D), radiolarians appear in high portion in samples 299, 332 and 338. The dominant *Calpionella alpina* with rare *Crassicollaria parvula* and *Tintinnopsella carpathica* with *Tint. doliphormis* create a calpionellid association typical of the Alpina Subzone. Calpionellids are accompanied by rare to seldom cysts of *Colomisphaera carpathica*, *Col. cieszynica* (Fig. 4H), *Col. lapidosa,* (Fig. 4I), *Col.* cf.

fortis, *Col.* sp., *Stomiosphaerina proxima* (Fig. 4J) and *Cadosina semiradiata semiradiata,* microproblematica of *Gemeridella minuta* (Fig. 4K) and *Didemnum carpaticum* (Fig. 4L).

Calpionella Zone, Ferasini Subzone
(*sensu* Remane et al. 1986)

Biomicrites, locally slightly bioturbated with calpionellid-*Globochaete*, calpionellid-*Globochaete*-radiolarian and radiolarian wackestones (studied in samples 340–343). In the calpionellid association *Calpionella alpina* dominated over the infrequent *Remaniella ferasini*, *R. catalanoi*, *R. durandelgai*, *R. borzai*, *Tintinopsella carpathica*, *Crassicollaria parvula*. The dinoflagellate cyst association consists of *Colomisphaera lapidosa*, *Col. carpathica*, *Stomiosphaerina proxima*, *Cadosina semiradiata fusca* and *Cad. semiradiata semiradiata*.
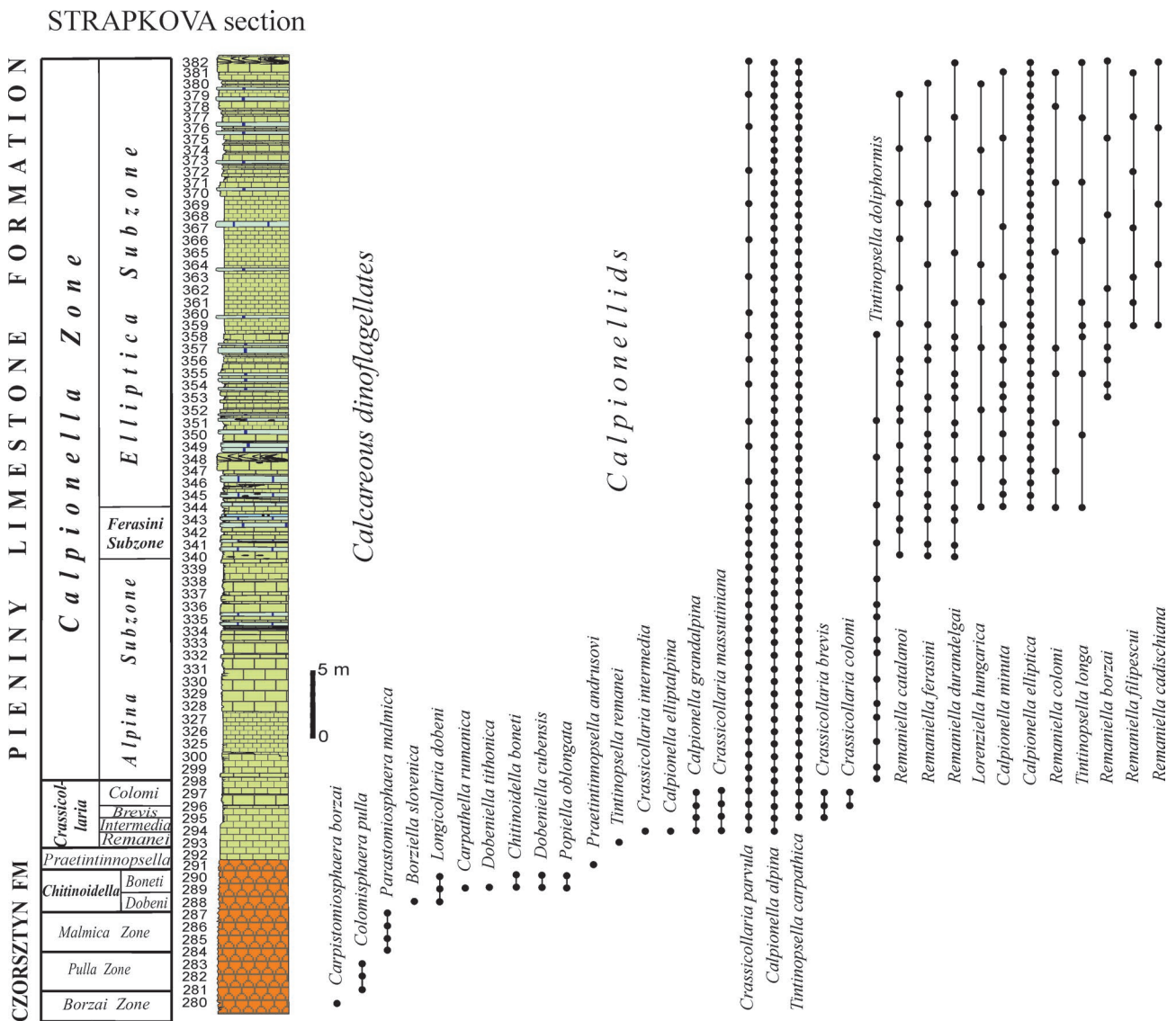

Fig. 7. Vertical range of calpionellid species and cysts of calcareous dinoflagellates.
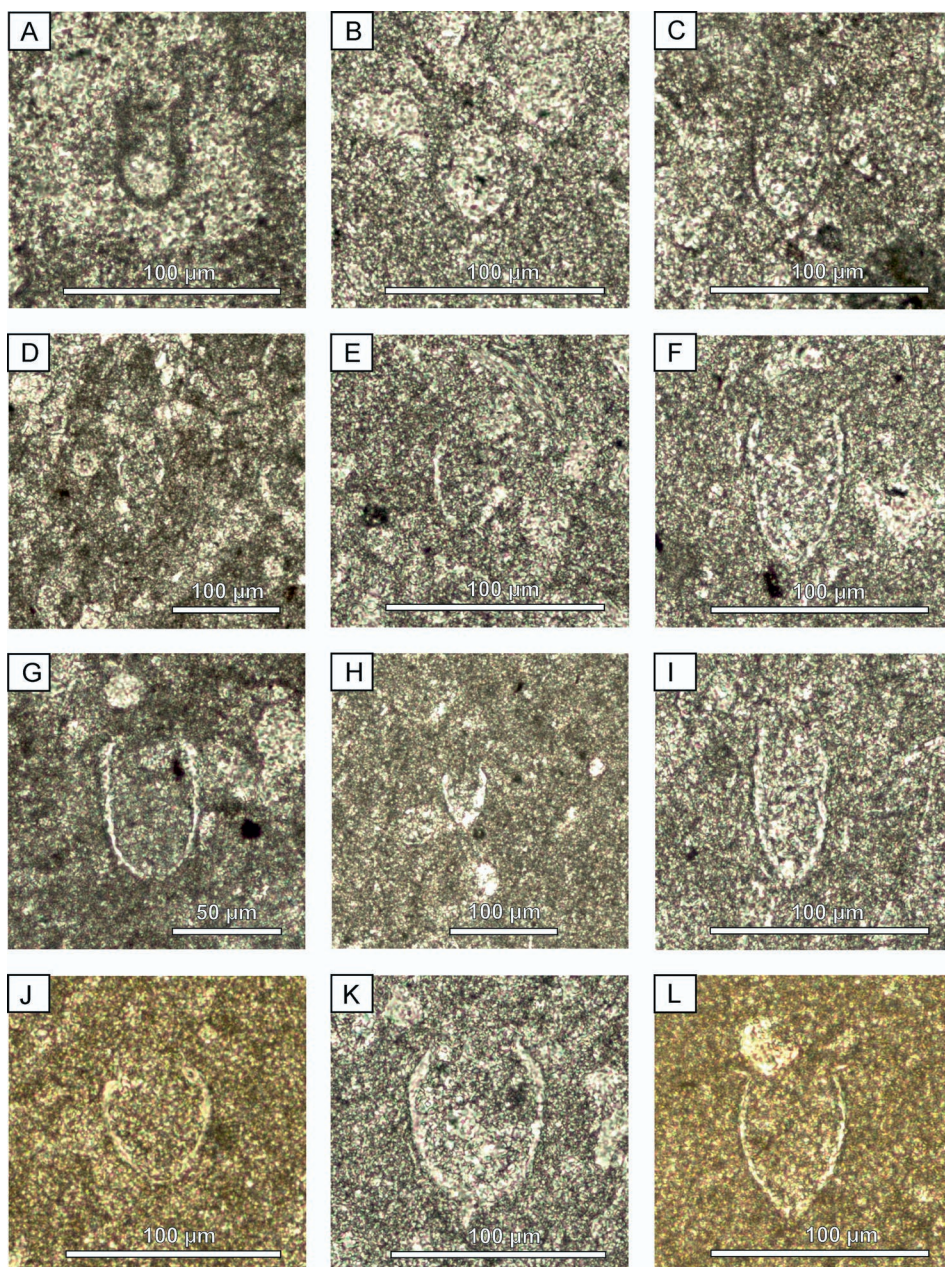
Fig. 8. Calpionellids in the Strapkova section: **A** — *Longicollaria dobeni* (Borza). Sample 288. **B** — *Chitinoidella boneti* Doben. Sample 290. **C** — *Chitinoidella elongata* Řehánek. Sample 289. **D** — *Tintinnopsella remanei* Borza. Sample 293. **E** — *Praetintinnopsella andrusovi* Borza. Sample 291. **F** — *Crassicollaria intermedia* (Durand Delga). Sample 294. **G** — *Crassicollaria massutiniana* (Colom). Sample 293. **H** — *Crassicollaria brevis* Remane. Sample 295. **I** — *Crassicollaria colomi* Doben. Sample 298.1. **J** — *Calpionella alpina* Lorenz. Sample 295. **K** — *Calpionella grandalpina* Nagy. Sample 294. **L** — *Tintinnopsella carpathica* (Murgeanu and Filipescu). Sample 347.

Calpionella Zone, Elliptica Subzone
(*sensu* Pop 1974)

Biomicrites, locally bioturbated wackestones (samples 344–359) with radiolarian-Calpionella-*Globochaete* and Calpionella-*Globochaete* microfacies contain calpionellid associations of *Calpionella alpina, Calp. elliptica* (Fig. 9B, C)*, Calp. minuta, Tintinopsella carpathica* (Fig. 9L)*, Tint. longa* (Fig. 9A)*, Lorenziella hungarica* (Fig. 9I)*, Remaniella catalanoi, Rem. ferasini* (Fig. 9D, E)*, Rem. durandelgai* (Fig. 9F),

Rem. borzai (Fig. 9H)*, Rem. colomi, Rem. filipescui, Rem. cadischiana* (Fig. 9G). Cysts are represented by *Colomisphaera lapidosa, Colom. carpathica, Cadosina semiradiata semiradiata* and *Cad. semiradiata fusca*.

Calcareous nannofossils and nannofossil zonation

In the samples studied, calcareous nannofossils are rather rare and their preservation ranges from moderate (only in a few samples) to extremely poor, heavily etched by dissolution. In total, 29 calcareous nannofossils taxa were indentified. A comparable diversity has been observed in the Barlya section (Lakova et al. 1999) and in the Nutzhof (Reháková et al. 2009). A slightly lower diversity has been reported from the Brodno (Michalík et al. 2009) and Hrušové sections (Ondrejíčková et al. 1993), conversely higher diversity and abundance also have been observed, for example, in the Puerto Escaño (Svobodová & Košťák 2016) or Torre de Busi and Foza sections (Casellato 2010). Successive distribution of nannofossils along the lithological column is shown in the Fig. 10. *Watznaueria* (more than 55 %), *Cyclagelosphaera* (nearly 20 %), *Conusphaera* (14 %), and *Nannoconus* (7 %) are the most abundant components of the assemblage (Fig. 10). The occurrence of these most abundant genera is in accordance with previous studies of calcareous nannofossils of the JKB interval (e.g., Michalík et al. 2009; Reháková et al. 2009; Lukeneder et al. 2010; Wimbledon et al. 2013). Nannoliths represented by *Polycostella beckmannii, Hexalithus noeliae* and *Assipetra infracretacea* are less present. The species indicative of eutrophic environments such as *Zeugrhabdotus erectus* and *Diazomatholithus lehmannii* occur only sporadically. Despite the poor preservation, several biostratigraphically important
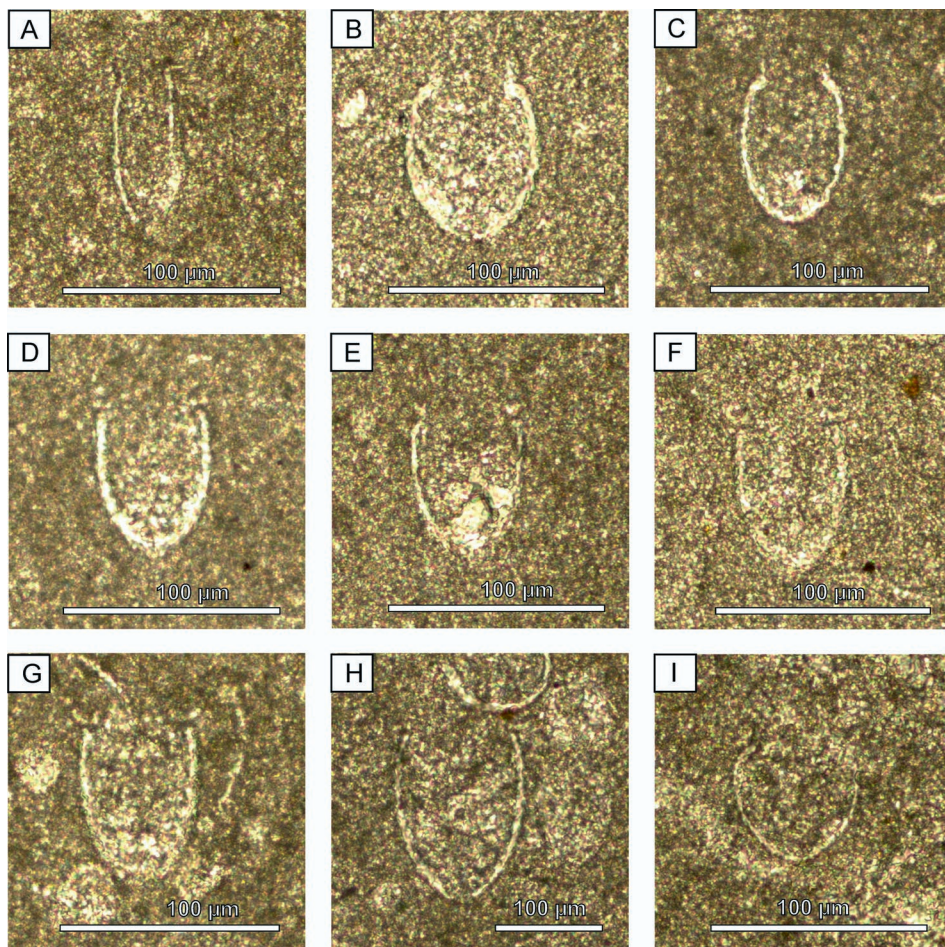
Fig. 9. Calpionellids in the Strapkova section: A — *Tintinnopsella longa* (Colom). Sample 345. **B, C** — *Calpionella elliptica* Cadisch. Samples 344; 359. **D, E** — *Remaniella ferasini* (Catalano). Sample 346; 354. **F** — *Remaniella durandelgai* Pop. Samples 344; 346. **G** — *Remaniella cadischiana* (Colom). Sample 359. **H** — *Remaniella borzai* Pop. Sample 353. **I** — *Lorenziella hungarica* Knauer and Nagy. Sample 343.

Bralower et al. (1989) was recorded in bed 352, in the lower part of the Elliptica Subzone (Fig. 10). *N. kamptneri kamptneri* was not found in the samples studied.

Geochemistry

Carbonate and C_{org} contents

The $CaCO_3$ content in the uppermost part of the Czorsztyn Fm. is relatively high (Fig.12). In the basal part of the Pieniny Fm. (from the beds 291 to 300) it decreases below 80 %. The decrease is in accordance with microfossil analysis which pointed to raised silica bioproduction. The $CaCO_3$ content reaches up to 90 % again in the Pieniny Fm. (325–360), where nannoconid and calcareous microplankton remnants become abundant (Tremolada et al. 2006; Michalík et al. 2009; Grabowski et al. 2013).

However, locally — as in bed 334 (Fig. 12), the $CaCO_3$ content decreases below 50 %. Microfacies study have suggested that the main source of silica in the whole sequence came from radiolarians and only a very low amount came from detrital minerals (quartz, clays, accessories; Figs. 2 and 5). Silica (opal–chalcedony) came from radiolarian tests, replaced by calcite and concentrated in cherts.

TOC content is low (0.08–0.31 %) in all samples (Fig. 12). The C_{org} contents slightly increases (more than 0.1 %) in the top of the Czorsztyn Fm and at the base of the Pieniny Fm., where $CaCO_3$ content decreases. Similarly, in beds 350 and 353, slight TOC accumulation could result from selective sorption of (dissolved) C_{org} by fine grains with more active surface, but probable also from raised fossil production.

Stable carbon and oxygen isotopes

Both C and O isotopes of bull rock samples show a relatively small variation and shift within a relatively narrow range (δ^{13}C range from +1.09 to +1.96 ‰ VPDB, δ^{18}O from −2.93 to −1.20 ‰ VPDB). Late Tithonian δ^{13}C values (+1.96 to +1.46 ‰ VPDB) show a slightly decreasing trend (Fig. 12). Next, higher up section (beds 188–300) values
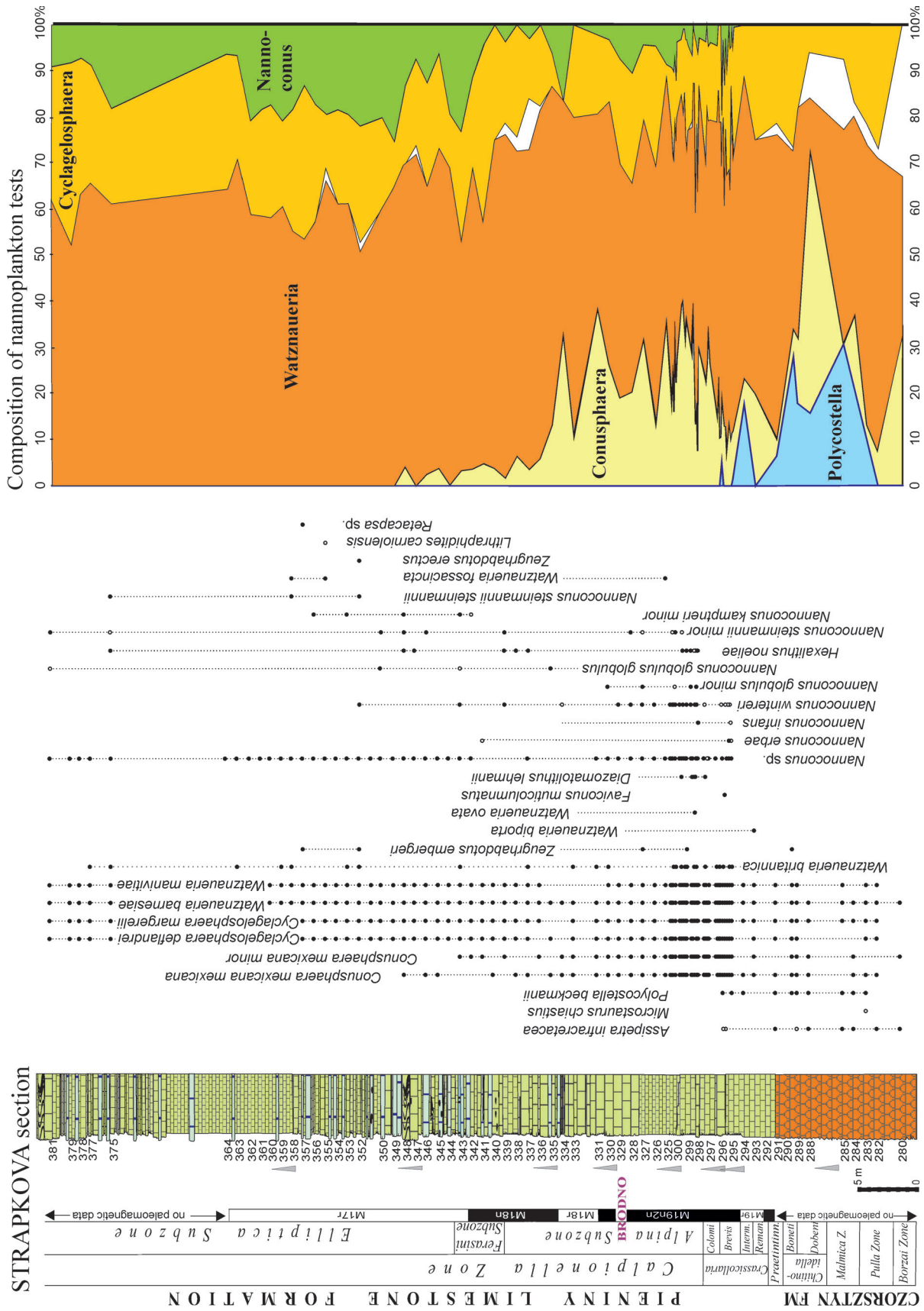
species have been recorded: *Nannoconus wintereri, N. steinmannii minor, N. kamptneri minor, N. steinmannii steinmannii*. The full list of calcareous nannofossil taxa found is given in alphabetical order in the "Appendix" and stratigraphically important taxa in the Fig. 11.

The abundance of calcareous nannofossils in the sequence is generally low. On average throughout the section, about 50 specimens per sample were observed. It means one specimen per six fields of view of the microscope. Due to the low abundance and prevailing bad preservation of calcareous nannofossils, only several biostratigraphic events have been defined. The first occurrence (FO) of *N. wintereri* was recorded in the bed 298.1, close to the expected JKB interval based on calpionellids (this study, see above). This bioevent represents the base of the NJT 17b Subzone, which Casellato (2010) considered to cover the JKB interval. The FO of *N. steinmannii minor* was recorded in bed 300.0 in middle part of the M19n magnetozone. Casellato (2010) indicates it as the base of the NKT Zone. *N. kamptneri minor* occurs sporadically from bed 343 upwards. The FO of *N. steinmannii steinmannii*, namely the base of the NK-1 Zone *sensu*

Fig. 10. Vertical ranges of nannofossils and quantitative distribution of nannoplankton genera (open circles indicate uncertain species identification).
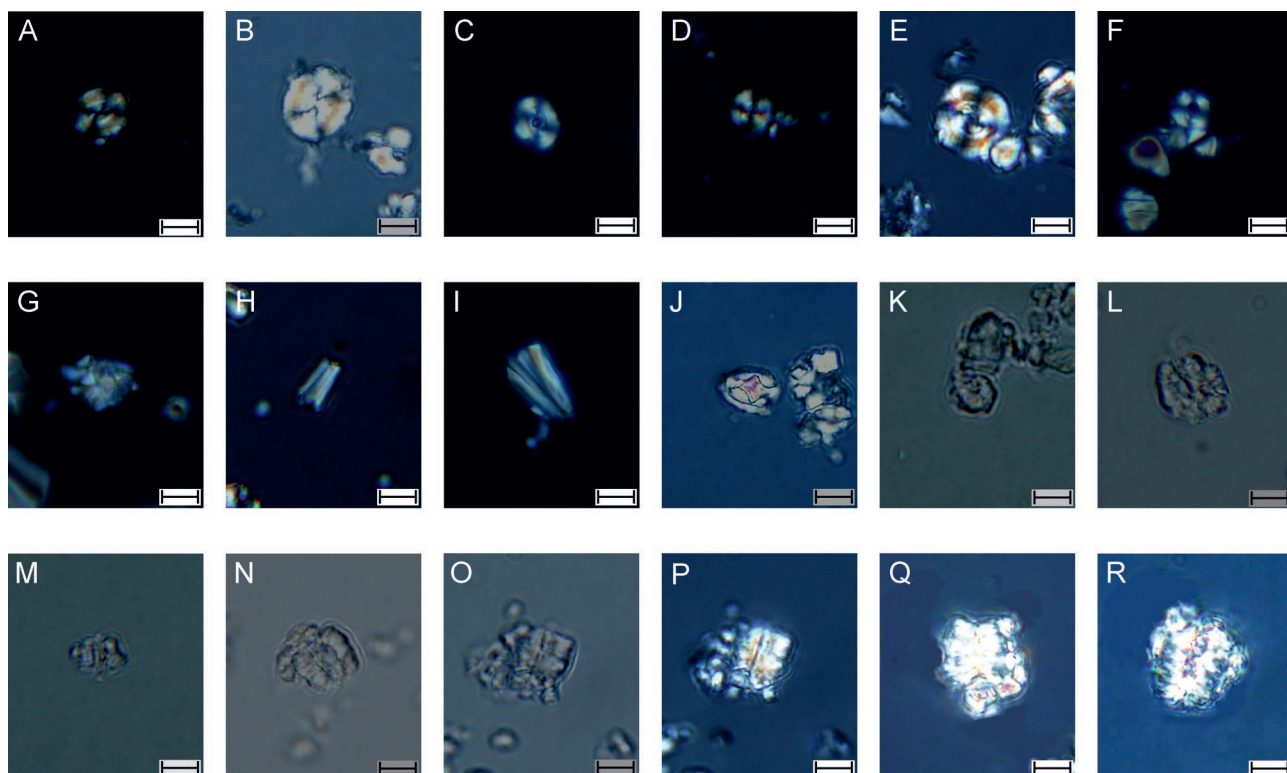
Fig. 11. Important nannofossils species. Scalebar represents 5 μm. **A** — *Watznaueria barnesiae* (Black in Black & Barnes) Perch-Nielsen. Sample 291. **B** — *Watznaueria manivitiae* (Bukry) Moshkovitz & Ehrlich. Sample 330. **C** — *Watznaueria britannica* (Stradner) Reinhardt. Sample 299.5. **D** — *Cyclagelosphaera margerelii* Noël. Sample 293. **E** — *Cyclagelosphaera deflandrei* (Manivit) Roth. Sample 300.1. **F** — *Diazomatolithus lehmanii* Noël. Sample 297.3. **G** — *Hexalithus noeliae* (Noël) Loeblich & Tappan. Sample 299.4. **H** — *Conusphaera mexicana* (Trejo) subsp. *minor* (Bown and Cooper) Bralower in Bralower et al. Sample 295. **I** — *Conusphaera mexicana* (Trejo) subsp. *mexicana* Bralower in Bralower et al. Sample 299.3. **J** — *Zeugrhabdotus embergeri* (Noël) Perch-Nielsen. Sample 298.4. **K** — *Nannoconus globulus* (Brönnimann) subsp. *minor* Bralower in Bralower et al. Sample 330. **L** — *Nannoconus globulus* (Brönnimann) subsp. *globulus* Bralower in Bralower et al. Sample 350. **M** — *Nannoconus wintereri* Bralower and Thierstein in Bralower et al. Sample 352. **N** — *Nannoconus kamptneri* (Brönnimann) subsp. *minor* Bralower in Bralower et al. Sample 356. **O** — *Nannoconus steinmannii* (Kamptner) subsp. *minor* Deres and Achéritéguy. Sample 300. **P** — *Nannoconus steinmannii* (Kamptner) subsp. *minor* Deres and Achéritéguy. Sample 300. **Q** — *Nannoconus steinmannii* (Kamptner) subsp. *minor* Deres and Achéritéguy. Sample 381. **R** — *Nannoconus steinmannii* (Kamptner) subsp. *steinmannii* Deres and Achéritéguy. Sample 358.

achieving a range of +1.14 to +1.38 ‰ (in average +1.24 ‰ VPDB) show a new (balanced) isotope C composition of marine water during sedimentation of the Pieniny Fm. The high resolution carbon isotope record resembles the typical (stable or smooth) trend worldwide documented in the J/K boundary sequence (Weissert & Mohr 1986; Weissert & Channel 1989; Weissert & Lini 1991; Gröcke et al. 2003; Tremolada et al. 2006; Žák et al. 2011; Price et al. 2016). The same δ^{13}C values between +1.3 to +1.5 ‰ (VPDB) occur in the Brodno (+1.3 to +1.6 ‰), Hlboča (+1.0 to +1.5 ‰), and Strážovce (+1.0 to +1.3 ‰) sections (Michalík et al. 1995; 2009). At the Nutzhof section that was also located on the north Tethyan margin (Lukeneder et al. 2010) which is in an equivalent position on the north Tethyan margin, bulk carbon isotope values range between +0.49 and +2.10 ‰.

The range of δ^{18}O data is not larger than 2 ‰, δ^{18}O values are relatively high in nodular limestones of the Czorsztyn Formation, and sharply decline at the onset of the Middle Tithonian. However, on average they remain close to 2 ‰ VPDB in the Pieniny Formation (Fig. 12). Although δ^{18}O

values strongly vary over small stratigraphic scales, namely between individual beds, they do not show clear large-scale trends. δ^{18}O values can be diagenetically modified more strongly than δ^{13}C. In the basal part of the Pieniny Fm (beds 292–300.6) δ^{18}O data shift from –1.48 to –2.48 ‰. δ^{18}O values in higher part of the section (325–360) reach –1.84 to –2.93 ‰.

Physical properties

Rock magnetism and demagnetization

Samples were moderately to weakly magnetic with NRM intensities in the lower part of the section (up to sample 335 including Tithonian and lower part of the Berriasian) mostly between 1 and 5×10^{-4} A/m. Sample 296.5 revealed the highest NRM intensity around 9.5×10^{-4} A/m. Higher up, in the upper part of the lower Berriasian, the NRM values fluctuated around 1×10^{-4} A/m (Supplementary Fig. S1).
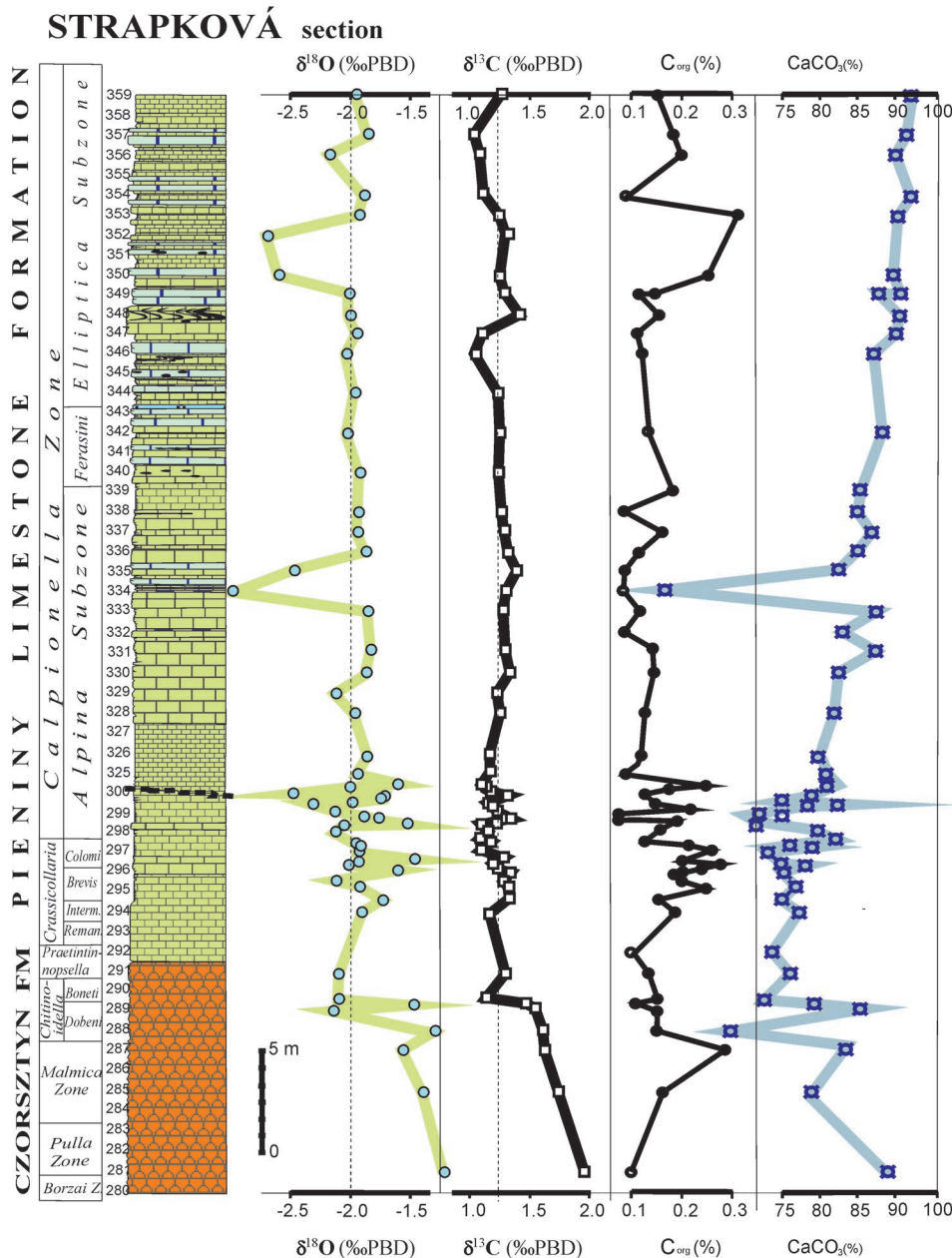
Fig. 12. Late Jurassic and Early Cretaceous C and O isotope stratigraphy calibrated against quantity of selected groups of microfossils and siliclastics.

sample. The maximum unblocking temperature of 640 °C unambiguously indicates the presence of hematite. Samples with moderately negative values of S-ratio (between −0.3 and −0.7) reveal presence of magnetite which is a dominant magnetic carrier. Its presence is documented by the maximum unblocking temperature of 520–560 °C in the 0.1T curve. However, the contribution of hematite is still significant as can be seen on the 1T curve (Supplementary Fig. S3B−D). Samples with low negative values of S-ratio contain almost exclusively magnetite (Supplementary Fig. S3E). It might be observed from the vertical log of S-ratio (Supplementary Fig. S1) that the contribution of hematite is slightly more distinct in the lower half of the section.

During thermal demagnetization, three characteristic NRM components were revealed. The least stable A component is unblocked between 20 and 150–200 °C (Fig. 13). An intermediate B component is demagnetized in the temperature range 200–420 °C. Finally, a double polarity C component might be identified between 420 and 480−520 °C. Unfortunately, abrupt MS rise is observed during thermal treatment between 400 and 450 °C (Fig. 13) and sometimes the C component cannot be demagnetized to the origin.

Age of magnetization components and palaeotectonic implications

The **A component** clusters match better in the present day coordinates (Table 1 and Fig. 14A). Their direction in geographic coordinates is close to the present day normal polarity geomagnetic field direction in the area of investigation. Therefore, they are interpreted as recent viscous remanent magnetization of no geological importance. The mixed polarity **C component** is interpreted as the primary one. After bedding correction, the normal (Cn) and reversed (Cr)

Low coercivity minerals dominate within the section which is manifested by negative values of S-ratio, mostly between −0.9 and −0.7 (Supplementary Figs. S1 and S2). Three samples (ST 333, 337.5 and 356.5) reveal slightly higher values of S-ratio: between −0.5 and −0.3. A single sample ST 296.5 reveals an extremely high value of S-ratio: 0.54. The sample 296.5 also contains an unusually large amount of ferromagnetic minerals which is manifested by a very high intensity of the IRM_{1T} (Supplementary Fig. S1). The sample 296.5 might also be distinguished by relatively high unblocking temperatures (up to 620 °C) and slightly different direction of C component (see below). Results of Lowrie's (1990) analyses (Supplementary Fig. S3A) confirm that medium and high coercivity minerals dominate in this
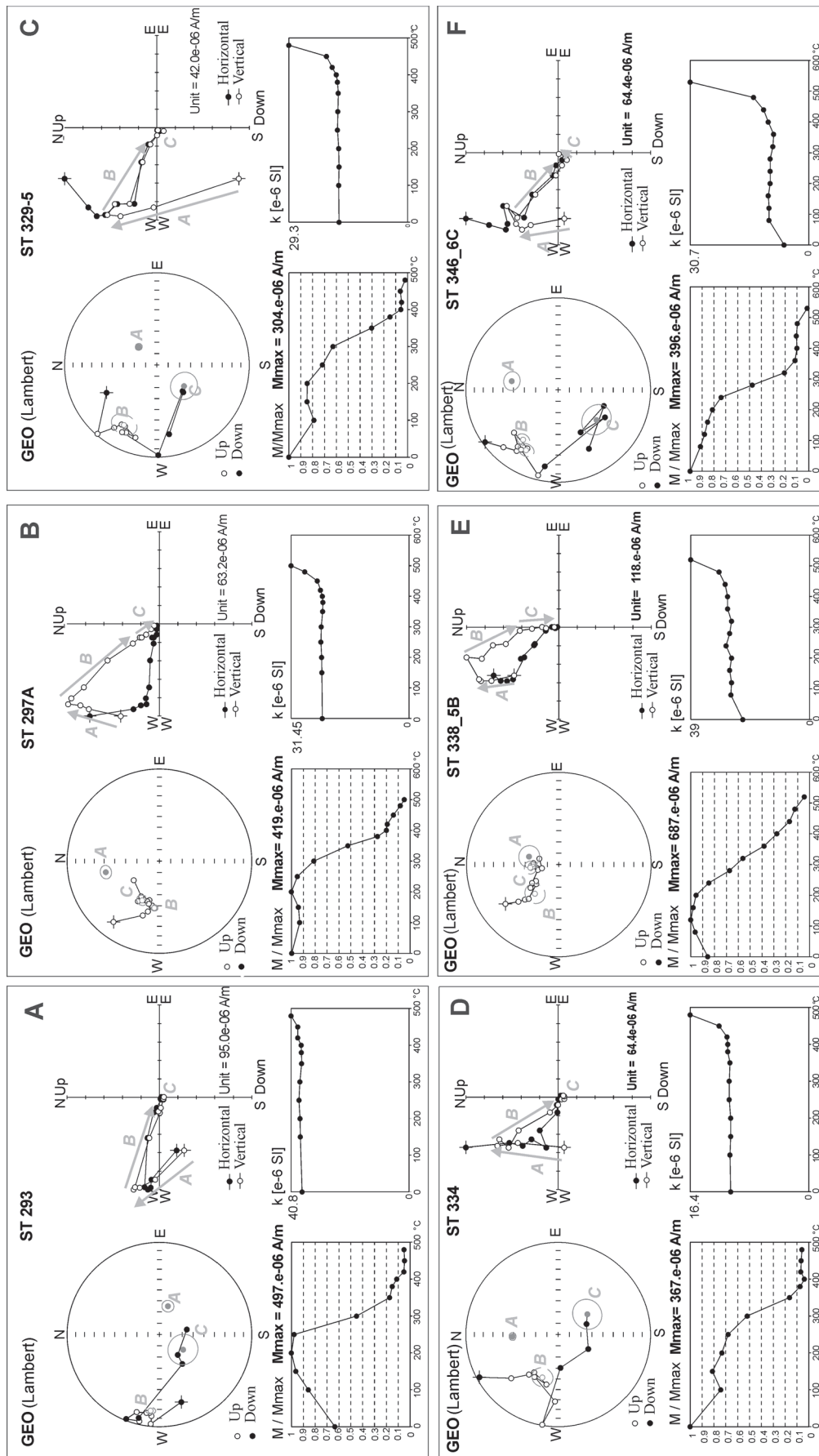
Fig. 13. Thermal demagnetization of typical specimens. Upper left: stereographic projection of demagnetization path; upper right: orthogonal projection; lower left: NRM decay during thermal treatment; lower right: MS changes during thermal treatment. Components A, B and C are indicated in stereographic and orthogonal projections. **A** — sample 293, Late Tithonian Crassicollaria remanei Subzone, M19r magnetozone; **B** — sample 297A, Late Tithonian Crassicollaria colomi Subzone, M19n2n magnetozone; **C** — sample 329_5, Early Berriasian Calpionella alpina Subzone, M19n1r ("Brodno") magnetozone; **D** — sample 334, Early Berriasian Calpionella alpina Subzone, M18r magnetozone; **E** — sample 338_5B, Early Berriasian Calpionella alpina Subzone, M18n magnetozone; **F** — sample 346_6C, Early Berriasian Calpionella elliptica Subzone, M17r magnetozone.

Table 1: Characteristic magnetizations from the Strapkova section. Palaeopoles: (Cn+Cr population) — Pole latitude: 44.6°N; Pole longitude: 268.2°E; dp=6.0, dm=10.1 (Cn+Cr selected population) — Pole latitude: 52.4°N; Pole longitude: 257.9°E; dp=5.1, dm=8.4 (dp, dm — confidence oval of palaeopole estimation). Explanations: **D/I** — declination/inclination before tectonic correction, **Dc/Ic** — declination / inclination after tectonic correction; **$α_{95}$, k** — Fisher statistics parameters, **N/No** — number of beds investigated/used for calculation of mean direction.

Component	D/I	$α_{95}$	k	Dc/Ic	$α_{95}$	k	N/No
A	4/62	5.1	13.42	65/-39	9.2	4.9	62/65
B	308/-42	8.9	5.09	351/73	8.8	5.15	62/65
Cn	324/-61	15.3	3.93	321/55	11.1	6.64	30/65
Cr	233/52	7.0	13.4	130/-24	10.6	6.33	34/65
Cn+Cr	213/59	7.6	6.44	314/39	8.5	5.39	64/65
Cn select	324/-62	9.7	10.31	335/55	8.2	14.06	24/65
Cr select	233/55	7.6	13.81	139/-28	8.3	11.82	28/65
Cn+Cr select	205/63	7.6	7.8	**325/41**	**6.9**	**9.16**	**52/65**

directions cluster in the NW and SE quadrant, respectively, of a stereonet with moderate inclination (Fig. 14C). Its primary nature is also supported by the fact that polarity changes of the C component correlate well with the Global Polarity Time Scale (see below). The clustering of the C component does not improve after tectonic correction (Table 1) as might be expected in the case of a primary component. The McFadden & McElhinny's (1990) reversal test gives negative results (critical angle 14.5°, $γ_c$=30.6°). It might be explained either by contamination of the intermediate B component or incomplete demagnetization of the samples containing hematite. The **B component** must be regarded as secondary magnetization, as it always reveals a normal polarity (Fig. 14B). Significant spread of both B and C components might result from overlapping of unblocking temperature spectra and from incomplete demagnetization of hematite. The position of the B component is usually close to Cn primary component (Table 1). Therefore, the B component most probably represents pre-folding or early synfolding remagnetization of normal polarity. It might be acquired during the maximum burial or early phase of Late Cretaceous folding and thrusting, alike abundant secondary magnetizations documented in the Central Western Carpathians (Grabowski 2005; Grabowski et al. 2009).

In the pre-folding coordinates, the declination of C component reveals a moderate 46° counter-clockwise (CCW) rotation from the present-day north (Table 1). However, clustering of the C component is too weak for significant palaeotectonic application (the value of precision parameter k >10 is required; see Van der Voo 1993). Having applied some selection (rejecting specimens deviating from the main cluster), the amount of the CCW rotation slightly decreases to 35°. Clustering of the C component (both normal and reversed populations) improves after tectonic correction, although the precision parameter k is still slightly below 10 (see Table 1 and Fig. 13d) and the reversal test is still negative. Declination of the C component is concordant with the general CCW of the study area. A counter-clockwise rotation of 47° (±18°) was reported by Márton et al. (2013) from the Upper Cretaceous pelagic marls in the PKB in the neighbouring locality of Vršatec.

Palaeoinclination of the Strapkova section (41°), corresponding to palaeolatitude 24°N ±5° is slightly shallower than Tithonian–Berriasian palaeoinclinations from the PKB and Central Carpathian reference sections (Márton et al. 2015) which results from incomplete cleaning of the primary C component.

Magnetostratigraphy and correlation with the Global Polarity Time Scale (GPTS)

According to the polarity of the C component, four normal (N1–N4) and four reversed polarity intervals (R1–R4) were documented (Fig. 15). Samples 292 and 292.5 revealed normal polarity of the C component (N1 interval). The subsequent four samples between 293 and 294.5 were of reversed polarity (R1 interval). The long normal polarity (N2) interval was indicated between 295 and 328.5. It is followed by quick polarity changes manifested by the R2 (329 and 329.5) and N3 (330) intervals. The sample 330.5 was of undefined polarity. Three distinct polarity intervals were distinguished in the upper part of the section: reversed R3 interval (samples 331.5–334), normal N4 interval (334.5–341.5) and reversed R4 (343–363.9) interval.

The N1 interval is interpreted as the topmost part of the M20n magnetozone (Fig. 15). It is situated between the Tithonian Praetintinopsella Zone and the bottom of the Remanei Subzone. R1 interval is correlated with the M19r magnetozone. It covers the Remanei and Intermedia subzones. The long normal N2 interval must be interpreted as the M19n2n. The boundary between Crassicollaria and Calpionella zones is usually situated within this magnetozone (for review, see Ogg et al. 1991; Grabowski 2011; Satolli et al. 2015). The short R2 and N3 intervals, in the lower part of the Alpina Subzone, are respectively correlated with the M19n1r ("Brodno") and M19n1n magnetosubzones. The R3 interval is interpreted as the M18r magnetozone. This magnetozone is situated entirely within the Alpina Subzone (Houša et al. 2004; Grabowski & Pszczółkowski 2006; Pruner et al. 2010). The next normal N4 interval is paralleled with the M18n. The boundary between the Alpina and Ferasini subzones falls in the upper part of this magnetozone. It is concordant with the FAD of *Remaniella ferasini* which is observed usually in the M18n magnetozone (Ogg et al. 1991; Houša et al. 2004). A long reversed R4 interval in upper part of the section is interpreted as the M17r. It starts in the middle part of the Ferasini Subzone and continues into the Elliptica Subzone. It is concordant with abundant data from Italian sections (Ogg et al. 1991) and from the Pośrednie sections (Grabowski & Pszczółkowski 2006), where the FO of *Calpionella elliptica* is observed also in the M17r magnetozone. The FO of *Remaniella cadischiana* is noted in the bed 359 (Fig. 9G). As this taxon usually appears in the upper part
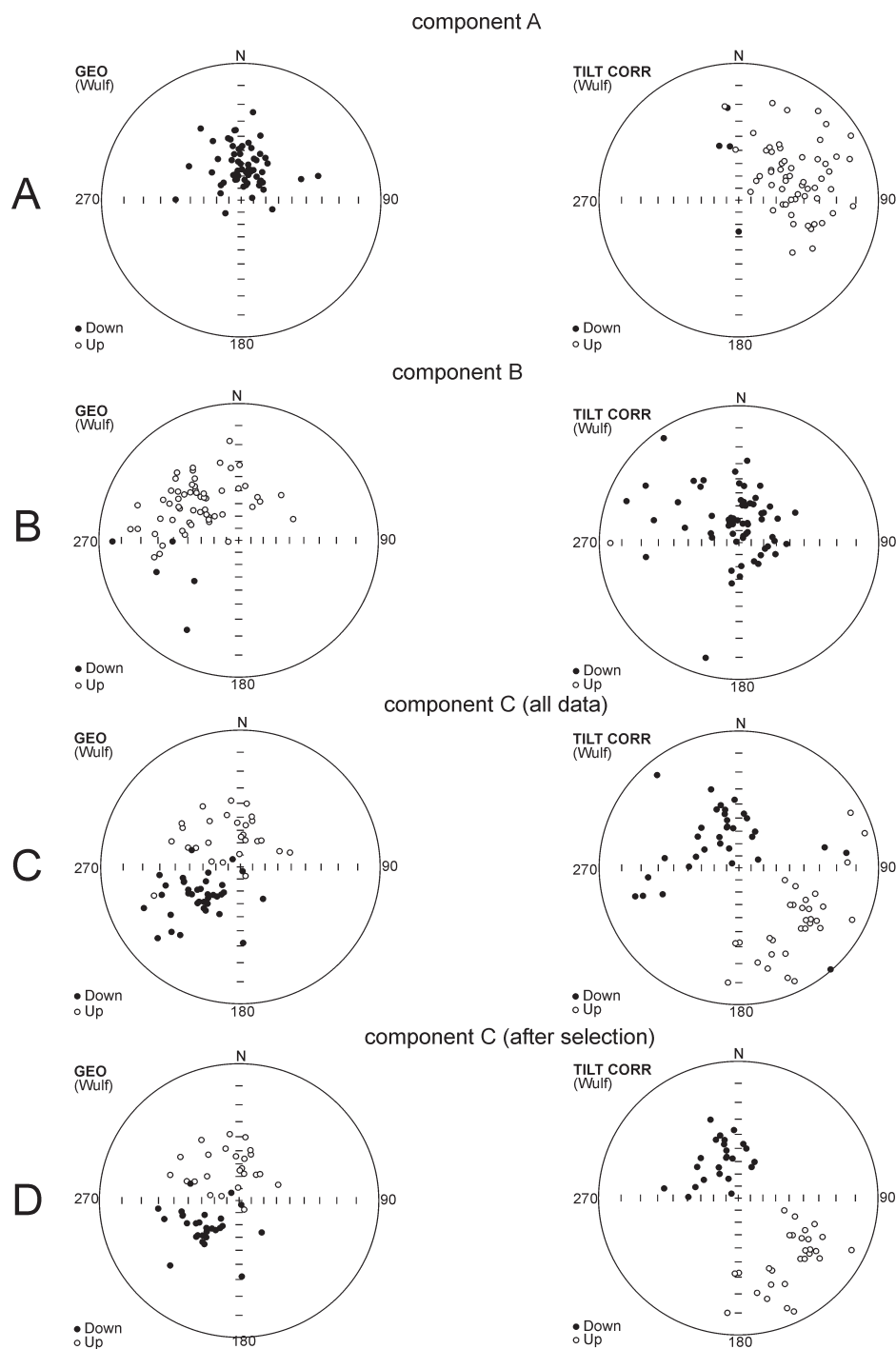
component A

component B

component C (all data)

component C (after selection)

be a significant contribution of ferromagnetic minerals to the MS. Although a long term decrease of the IRM_{1T} is observed as in the case of the MS (Supp. Fig. S1), the two curves are not identical which indicates that the contribution of paramagnetic minerals to MS cannot be neglected.

Magnetic susceptibility reveals a long term decreasing trend (Supplementary Fig. S1 and Fig. 16). Its values are relatively high in the lower half of the section, between $8-16 \times 10^{-9}$ m³/kg in the Tithonian and lowermost Berriasian (the Alpina Subzone, up to sample 338). Large MS variations are also observed in that part of the section. The MS decreases by 50 % throughout the Tithonian, up to the JKB. Then it fluctuates between 4 and 10×10^{-9} m³/kg in the lower part of the Alpina Subzone, in M19n and M18r magnetozones. Significant increase up to 12×10^{-9} m³/kg is observed in upper part of the Alpina Subzone, in the bottom part of the M18n magnetozone. Then MS again decreases throughout the M18n magnetozone to 4×10^{-9} m³/kg. Within the Ferasini and Elliptica Subzones, MS values gently fall from 4 to 3×10^{-9} m³/kg, with only two minor positive excursions in the M17r magnetozone.

Discussion

Environmental proxies

In contrast to other Mesozoic system boundaries, the JKB time span was related to less dramatic environmental changes, generating problems with the definition of the JKB position, reflected in contradictions of its determination in the Brodno and Strapková sections (Fig. 17) but also in its definition worldwide (Lukeneder et al. 2010; Michalík & Reháková 2011; Wimbledon et al. 2013; Schnabl et al. 2015; Price et al. 2016). Use of complex proxy parameters is inevitable.

Fig 14. Stereographic projections of the magnetization components A, B and C. Left column: before tectonic correction (*in situ*); right column: after tectonic correction (in bedding coordinates). Full symbols – lower hemisphere projection; open symbols – upper hemisphere projection.

of the M17r (Grabowski & Pszczółkowski 2006; Grabowski et al. 2010), it seems that the top of the section is quite close to the M17r/M17n magnetozones boundary.

Magnetic susceptibility

There is a moderately good correlation of MS with IRM (Supplementary Fig. S2A, B). This indicates that there might
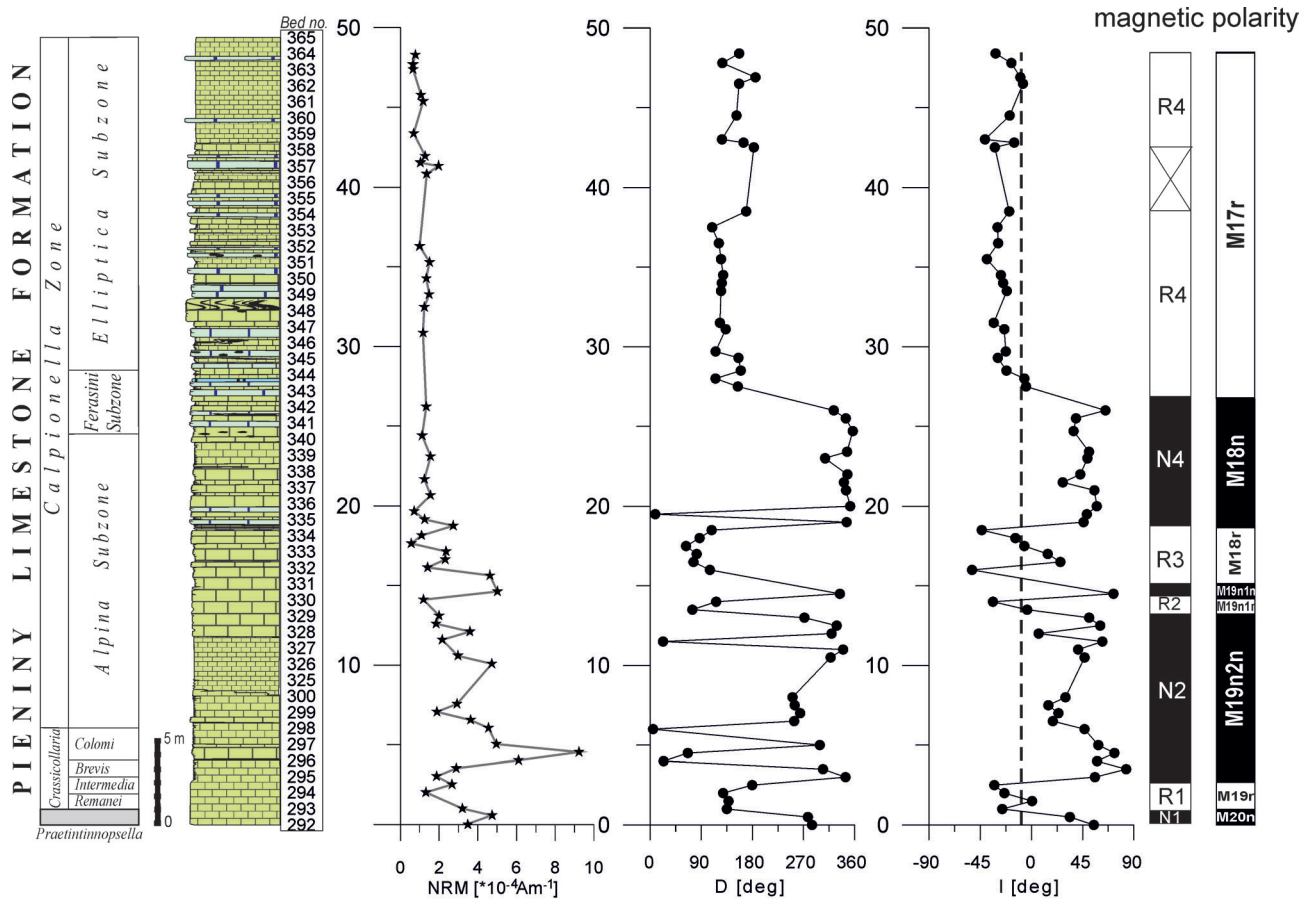
Fig. 15. Magnetostratigraphy (NRM intensity; declination — D; inclination — I of the component C).
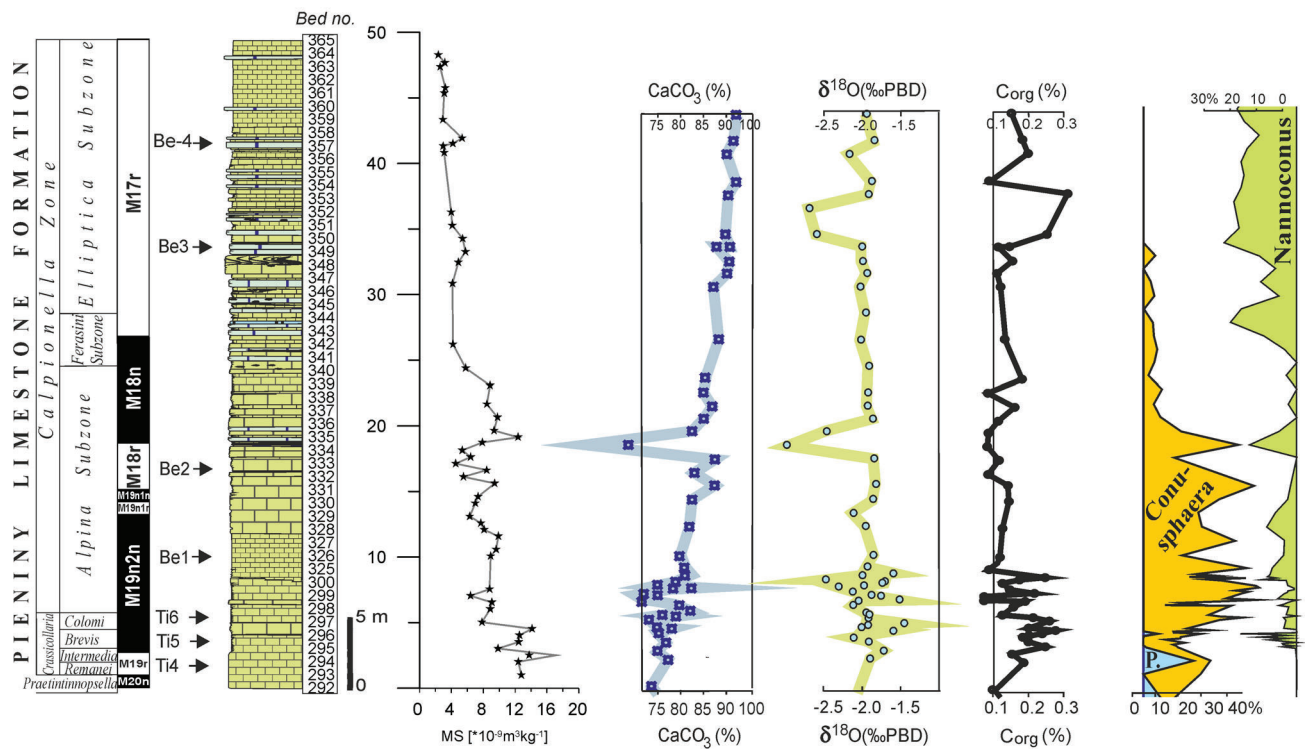

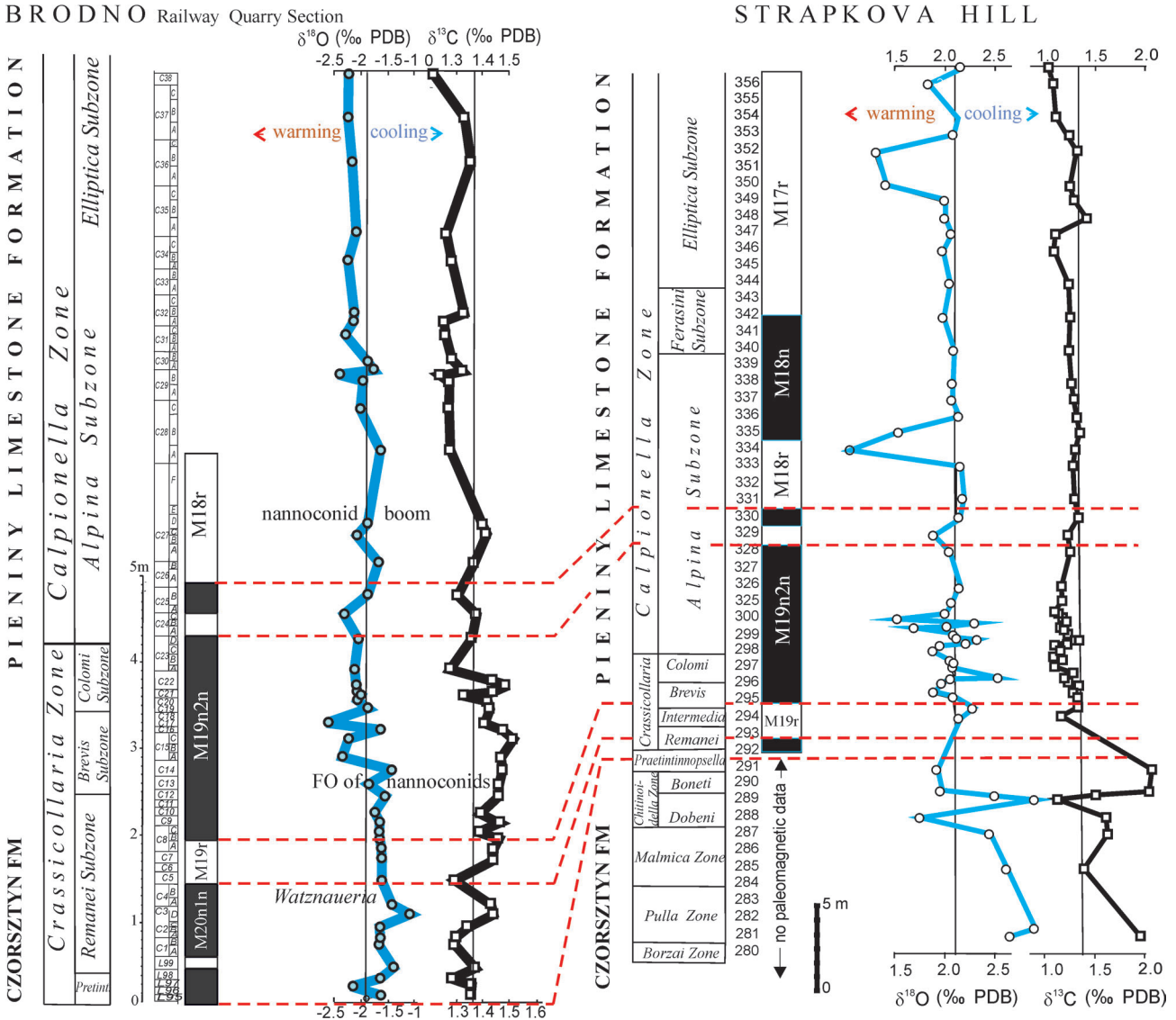**Fig. 16**. Final summarization of data from the Strapkova section.

Fig. 17. Integrated correlation of the O and C isotopes curves between Strapkova and Brodno sections.

Fluctuations of O isotope composition and distribution of nannoliths in "Maiolica-type" limestone, where sedimentary record, including C isotope composition, has not been influenced by clastic input, can closely reflect original environmental conditions.

A link between the abundance of calcareous nannofossils and the $CaCO_3$ content can be observed. The calcareous nannofossils abundance noticably increases from bed 298.6 and this trend continues up to the bed 299.6. This is an interval with the highest nannofossil abundance in the succession studied. This peak is associated with a higher $CaCO_3$ content (Figs. 12, 16). Conversely, the lowest calcareous nannofossil abundance has been recorded in bed 334, with only six specimens. This event correlates with the most remarkable decrease of the $CaCO_3$ content, with the radiolarian event and with the negative $\delta^{18}O$ excursion (Figs. 12, 16).

The observed shift in the $\delta^{18}O$ values (2 ‰) throughout the section could indicate a relatively strong temperature change

in the Early Cretaceous ice-free world (Anderson & Arthur 1983; Gröcke et al. 2003; Shurygin et al. 2015) in the JKB sequence upwards. However, the $\delta^{18}O$ signal can have been modified by other characteristics of water in the basin and by diagenetic processes in sediment. Bulk-rock analyses can be rather informative about relative changes in temperature and seawater $\delta^{18}O$ composition (Michalík et al. 2009; Lukeneder et al. 2010, 2015).

The shifts between samples are frequently smaller than 0.5 ‰ (Fig. 12). The first shift that occurred between the top of the Ammonitico Rosso and base of the Maiolica beds is relatively large (−1.20 to −2.18 ‰) and could indicate relatively continual and intensive temperature rise by 3.5 to 4 degree over a relative short (185–191 m) interval. The $\delta^{18}O$ signal is more stable (−1.48 to −2.15 ‰) at the JKB interval (192–300.6 m) and suggests stabilization of possible higher temperature values. Data obtained by detailed study of 25 samples fluctuate in a narrower interval (less than 0.7 ‰)

do not show any clear trend and imply a stable temperature regime at the J/KB. Negative δ^{18}O trend in the Maiolica sequence (325–360 m) continued and it indicates graded warming (approx.1–2.5 degree). Similar δ^{18}O trend and temperature range has been observed in the Brodno (Michalík et al. 2009) or in the Nutzhof sections (Lukeneder et al. 2010) or other section (Žák et al. 2011, Price et al. 2016).

Analysis of the data introduced above enabled stratigraphical and palaeoecological correlation of the Strapkova and Brodno sections (Fig. 17). Bed to bed fluctuation of δ^{18}O coincides with nanno- and microplankton events. During the Late Tithonian, an increase of *Polycostella* and *Conusphaera* was recorded. Increasing abundance of *Nannoconus* occurred during the Early Berriasian. Nannoconid peaks (beds 300; 334; 350–352) correspond to negative δ^{18}O excursions and higher calcite accumulation (Fig. 16). Nannoconids are regarded as warm-water taxa (Street & Bown 2000; Melinte & Mutterlose 2001; Tremolada et al. 2006; Michalík et al. 2009; Svobodová & Košťák 2016). According to the O isotope data, changes in calcareous nannofossil assemblage composition and the appearance of *Nannoconus*, *Polycostella* and *Conusphaera* (Figs. 10, 16) were followed by warming of 2–3 °C. On the other hand, the abundance of radiolarian tests indicates colder oxygenated and eutrophic upwelling intervals. Occasional colonization of hemipelagic bottom by infaunal trace maker assemblage indicates that the bottom water layer was not stagnant but periodically affected by contour intermediate and low velocity currents. Hüneke & Stow (2008) characterized contourite beds by fine lamination and remnants of micro-cross-lamination of silty particles, dominance of skeletal fragments of planktonic organisms, paucity of benthic shells, thorough bioturbation and burrowing of the underlying layer, dominance of microfacies of packed biomicrites, including wackestones and (foraminiferal) packstones, calcilutites with calcisiltite lenses, and so similar to the situation observed in the Strapkova section. The contourites should have been deposited on the foot of continental slope at a depth of more than 300 metres. Enhanced water dynamics could be responsible for microfossil redeposition and for several apparent blooms of crassicollarians. Temperature, salinity changes and raised trace metal contents in sea water could result in thinning and deformation of crassicollarian loricas (Tappan 1993; Reháková 2000b; Vandenbroucke et al. 2015) observed in several beds (296.3–297 m).

Sedimentation rate

The overall sedimentation rate increases up section, from 7.7 m/Myr in magnetozone M19r, through 9.5–9.8 m/Myr in M19n and M18r to 12.7 m/Myr in M18n and at least 15 m/Myr in M17r (see Table 2). This trend is in agreement with the data of Grabowski & Pszczółkowski (2006), who also documented an increasing sedimentation rate between the magnetozones M19r and M17r in the Pośrednie section (Fig. 18). Sedimentation rate in the Strapkova section is generally higher than in the Pośrednie section although the

Table 2: Attempt of sedimentation rate estimation in the Strapkova section (timescale after Ogg, 2012).

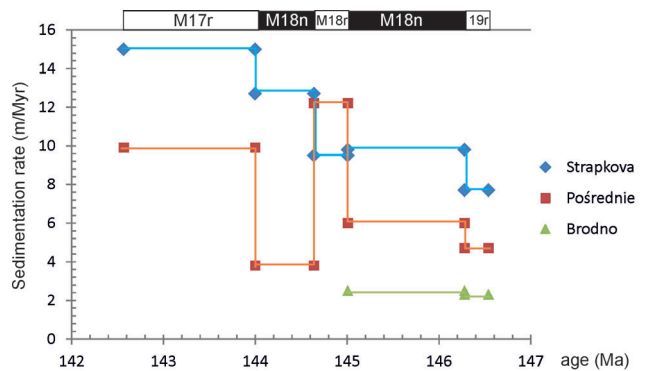| Magnetozone	Interval (m)	Thickness (m)	Duration (My)	Sedimentation rate (m/My)
M17r	48.4–26.75	21.65	1.44 (142.57–144.0)	15.0 (at least)
M18n	26.75–18.75	8	0.63 (144.0–144.63)	12.7
M18r	18.75–15.25	3.5	0.37 (144.64–145.01)	9.5
M19n	15.25–2.75	12.5	1.27 (145.01–146.28)	9.8
M19r	2.75–0.75	2	0.26 (146.28–146.54)	7.7

Fig. 18. Sedimentation rates in the Strapkova section compared with the Brodno section (PKB) and Pośrednie section (Tatra Mts., Fatric succession).

shape of curves does not exactly coincide (Fig. 18). It is also much higher than in the Brodno section, where it does not exceed 3 m/Myr in the M19r and M19n magnetozones (Houša et al. 1999). Compared with the South Alpine sections, the sedimentation rate in the Strapkova section is comparable to that in the Torre de Busi section in the Lombardian Basin (Channell et al. 2010; Grabowski 2011). It is higher than the sedimentation rate calculated for Trento Plateau sections (mostly 2–6 m/Myr in the M19r–M18n interval). It could indicate a more distal depositional setting of the Strapkova section in comparison with the Brodno section (Fig. 18).

Magnetic susceptibility and stratigraphic correlations

Magnetic susceptibility in pelagic and hemipelagic carbonates of Late Tithonian–Berriasian age is usually confined to lithogenic influx into a basin (Grabowski et al. 2013; 2014). This is most probably also the case in the Strapkova section, although geochemical data (e.g., correlation between lithogenic elements and MS) are not available. The MS curve obtained in the Strapkova section might be well correlated with coeval intervals in the Brodno section (Houša et al. 1999) and in the Pośrednie III section from the Tatra Mts. (Grabowski et al. 2013). A long term decreasing MS trend between the Upper Tithonian and upper part of the Lower Berriasian (i.e. top of M20n and M17r) is well constrained in the Pośrednie and Strapkova sections (Fig. 19). A part of this trend is also observed in the Brodno section between M19r and M18r. Short-term MS fluctuations might be compared as well.
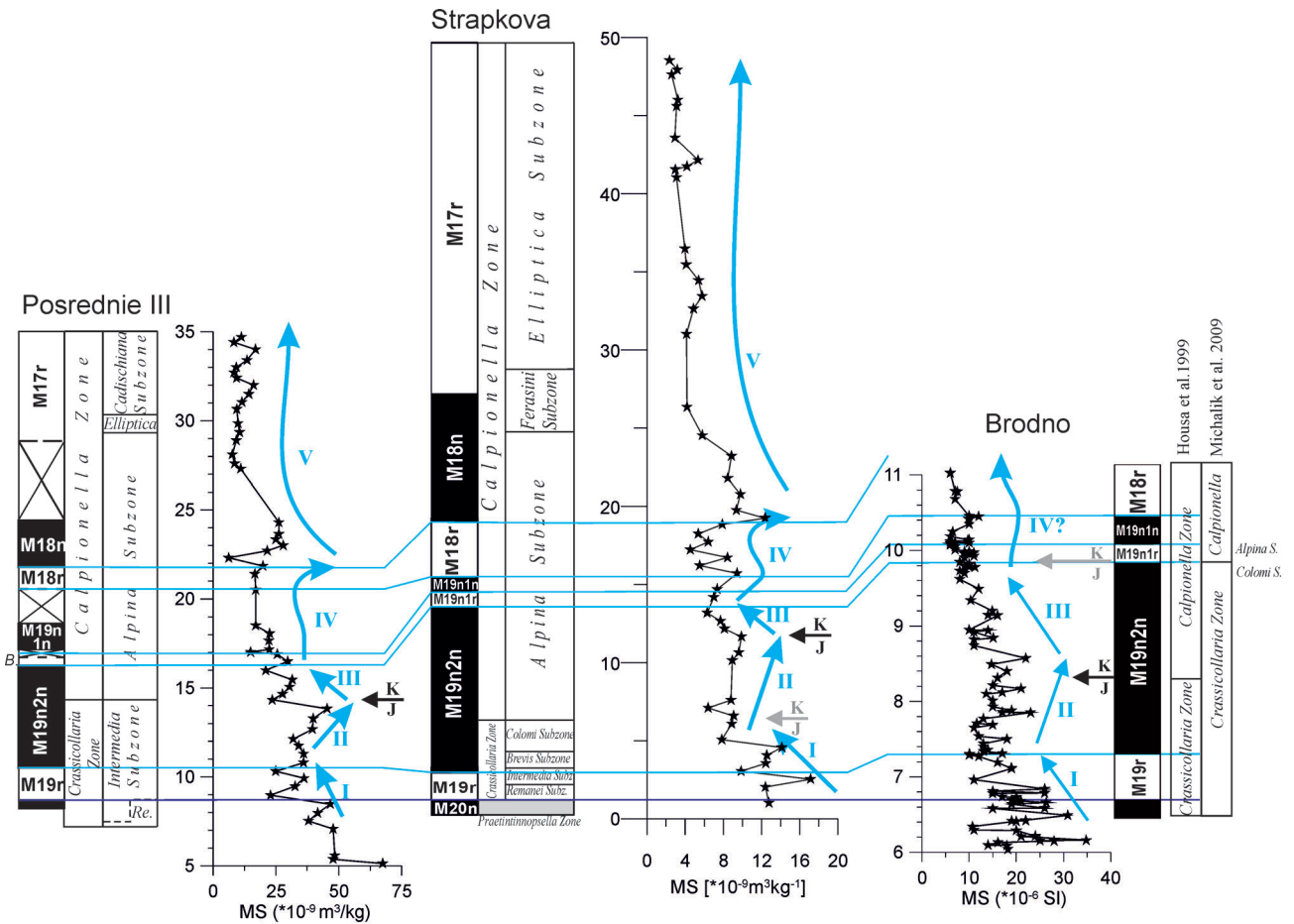
Fig. 19. Integrated correlation between Strapkova, Brodno and Pośrednie III sections based on bio-, magnetostratigraphy and magnetic susceptibility. Position of the Jurassic/Cretaceous boundary is indicated according to different definitions: black arrow - Intermedia/Alpina subzonal boundary; gray arrow - Colomi/Alpina subzonal boundary. Trends in MS variations (Roman numerals) are explained in the text.

A decreasing **trend I** occurs between the uppermost part of M20n, through M19r to the lower part of M19n2n. It is followed by a gently increasing **trend II**, which terminates in the upper part of M19n2n in the Strapkova and Pośrednie sections and in the middle part of this magnetozone in the Brodno section. Trend II in the Pośrednie III and Brodno sections terminates exactly at the J/K boundary, but in the Strapkova section — in the lower part of the Alpina Subzone.

The next decreasing **trend III** falls in the uppermost part of M19n2n, approximately up to the M19n1r (Brodno) magnetozone. **Trend IV** reveals a generally increasing character and culminates in a local MS maximum in the magnetozone M18n. It is well resolved in the Strapkova and Pośrednie sections, while most probably only the lowermost part of this trend is observed in the Brodno section.

Trend V is related to profound MS decrease in the upper part of M18n and in M17r, covering the uppermost part of the Alpina Subzone, through the entire Ferasini Subzone and a large part of the Elliptica Subzone. Trends I–V are apparently synchronous in relation to magnetostratigraphy. They might reflect changes of detrital input to the Pieniny and Zliechov (Central West Carpathians) basins controlled by regional tectonics and/or climate (Michalík 2007). The third, eustatic component (Grabowski et al. 2013), can be

involved after thorough correlation of well-dated but geographically remote sections.

MS variations in the Strapkova section negatively correlate with CaCO$_3$ content (see Fig. 16). The CaCO$_3$ increase between beds 292 and 333 matches well the MS decrease (trends I to III and the lower part of trend IV). The upper part of trend IV (with maximum MS values in lower part of M18n) might be compared with a slight decrease of CaCO$_3$ (beds 334 to 337). The final decrease of MS during trend V correlates exactly with increasing CaCO$_3$ in the uppermost Alpina, Ferasini and Elliptica subzones. Comparison of MS trends with nannofossil data (Fig. 16) indicates climatic control of MS variations. The abundance of *Conusphaera* (relative cooling) coincides with the high MS values of trends I to IV. The Nannoconus dominance (relative warming) is related to decreasing MS trend (trend V). Notably, the MS also correlates with sequence stratigraphy. Sequence boundaries and total plankton abundance maxima match with local MS highs (see Figs. 5a and 16).

There is an apparent contradiction between magnetic stratigraphy and biostratigraphy especially in the detailed situation of the JKB. It might be related to the fact, that the JKB was defined according to slightly different criteria. In the Pośrednie III (Grabowski & Pszczółkowski 2006) and

Brodno sections (Houša et al. 1999), the boundary was defined as the Intermedia/Alpina subzonal boundary. Alternatively, the Colomi/Alpina subzonal boundary was selected as the JKB marker in a revised version of the Brodno (Michalík et al. 2009) and in the Strapkova (this study) biostratigraphy. The Colomi/Alpina subzonal boundary is correlated with the top-most part of M19n2n (Michalík et al. 2009) in the Brodno section, but in the Strapkova section with its lower half. According to defined MS trends, the Colomi/Alpina boundary falls at the boundary between trends III and IV in the Brodno section and between trends I and II in the Strapkova (Fig. 19) section. The Intermedia/Alpina subzonal boundary is apparently synchronous in the Pośrednie and Brodno sections. It is situated in M19n2n, almost exactly between trends II and III, close to the local MS maximum. However, more high-resolution MS curves are desired, in order to test if the MS trends observed are also present in other sections beyond the Zliechov and the Pieniny basins.

Conclusions

The high-resolution analysis of calpionellid and dinoflagellate associations was used in order to characterize the JKB interval in the Strapkova section. Three dinoflagellate and four calpionellid zones have been recognized. They show a Late Tithonian burst and calpionellid diversification and a later decrease in diversity of crassicollarians. Such changes in plankton composition and diversity across the Jurassic/Cretaceous boundary were also documented by Reháková (2000), Reháková in Michalík et al. (2009), Wimbledon et al. (2013), Grabowski et al. (2010). The onset of the Alpina Subzone of the standard Calpionella Zone, used as a marker for the JKB, was documented in sample 298. This limit is defined by morphological change of *Calpionella alpina* tests. There, medium-sized spherical forms of *Calpionella alpina* dominate in biomicrite limestone and are accompanied by calcified radiolarians. The successive Ferasini Subzone characterized by the FO of *Remaniella ferasini* was identified in sample 340. In sample 344, *Calpionella elliptica*, the biomarker of the Elliptica Subzone appeared.

Nannofossil distribution documents the Tithonian NJT 17b Subzone to Early Berriasian NKT and NK-1 nannofossil zones (*sensu* Casellato 2010; and Bralower et al. 1989). The first occurrence of *Nannoconus wintereri*, which indicates the beginning of the NJT 17b Subzone and at the same time the beginning of the JKB transition has been located in sample 298.1.

Correlation of calcareous microplankton with C and O stable isotopes and TOC/$CaCO_3$ data distribution was used in characterization of the JKB interval. $\delta^{13}C$ values ranging from 1.1 to 1.4 ‰ (PDB) indicated a typical balanced regime of carbon in the sea water. Negative $\delta^{18}O$ shift from −1.5 to −2.3 ‰ (V-PDB) in the uppermost Tithonian indicates a temperature rise of 2−3° followed by stable temperature regime during the JKB with a warming tendency higher up the

section. Radiolarian laminites interpreted as contourites and bioturbation levels prove oxygenation events of bottom waters during the Berriasian.

Primary magnetization of mixed polarity was isolated and correlated with the Global Polarity Time Scale. The lower part of the Crassicolaria Zone (up to the middle part of the Intermedia Subzone) correlates with the M19r magnetozone. The M19n magnetozone includes the upper part of the Crassicollaria Zone and lower part of the Alpina Subzone. The reversed Brodno magnetosubzone (M19n1r) was identified in the uppermost part of M19n. The tops of the M18r and M18n magnetozones are located in the upper part of the Alpina Subzone and in the middle part of the Ferasini Subzone, respectively. The Ferasini/Elliptica subzonal boundary is located in the lowermost part of the M17r magnetozone.

General MS decrease between the upper Tithonian and Berriasian is in agreement with the increasing content of $CaCO_3$ and warming trend documented by nannofossils. It is also accompanied by an increasing sedimentation rate resulting from higher carbonate productivity.

It appears that the MS might be of some importance in precise correlation of calpionellid bioevents. Minor MS variations in magnetozones M19r and M19n, related to changes of detrital input, correlate between sections from the Pieniny Klippen Belt (Strapkova and Brodno sections) and Tatra Mts (Pośrednie section). They clearly demonstrate a subtle diachronism between Crassicollaria/Calpionella zonal boundaries, defined according to different criteria.

References

Andreini G., Caracuel J.E. & Parisi G. 2007: Calpionellid biostratigraphy of the Upper Tithonian–Upper Valanginian interval in Western Sicily (Italy). *Swiss J. Geosci.* 100, 179–198.

Anderson T.F. & Arthur M.A. 1983: Stable isotope of oxygen and carbon and their application to sedimentologic and environmental problem. In: Arthur M.A., Anderson T.F., Kaplan I.R., Veizer J. & Land L.S. (Eds.): Stable isotopes in sedimentary geology. *Soc. Econ. Paleont. Mineral. Short Course Note* 10, 1.1–1.151.

Bacelle L. & Bosellini A. 1965: Diagrams for visual estimation of percentage composition in sedimentary rocks [Diagrammi per la stima visiva della composizione percentualle nelle rocce sedimentarie]. *Ann. Univ. Ferrara, N. S., sez. IX., Sci. Geol. Paleont.* 1, 59–62 (in Italian).

Borza K. 1984: The Upper Jurassic–Lower Cretaceous

parabiostratigraphic scale on the basis of Tintinninae, Cadosinidae, Stomiosphaeridae and other microfossils from the West Carpathians. *Geol. Zbor. Geol. Carpath.* 35, 2., 539–550.

Boughdiri M., Sallouhi H., Maâlaoui K., Soussi M. & Cordey F. 2006: Calpionellid zonation of the Jurassic–Cretaceous transition in north Atlasic Tunisia. Updated Upper Jurassic stratigraphy of the "Tunisian Trough" and regional correlations. *Comptes Rendus Geosci.* 338, 1250–1259.

Bralower T.J., Monechi S. & Thierstein H. R. 1989: Calcareous nannofossils zonation of the Jurassic–Cretaceous boundary interval and correlations with the Geomagnetic Polarity Timescale. *Mar. Micropaleont.* 14, 153–235.

Casellato C.E. 2010: Calcareous nannofossil biostratigraphy of Upper Callovian–Lower Berriasian successions from the Southern Alps, N Italy. *Riv. Ital. Paleont. Strat.* 116, 3., 357–404.

Chadima M. & Hrouda F. 2006: Remasoft 3.0 — a user-friendly paleomagnetic data browser and analyzer. In: New Trends in Geomagnetism. Abstracts of the 10th "Castle Meeting". Castle of Valtice, September 3–8, 2006. *Travaux Geophysiques* 27, 20–21.

Channell J.E.T., Casellato C.E., Muttoni G. & Erba E. 2010: Magnetostratigraphy, nannofossil stratigraphy and apparent polar wander for Adria–Africa in the Jurassic–Cretaceous boundary interval. *Palaeogeogr. Palaeoclimatol. Palaeoecol.* 293, 51–75.

Grabowski J. 2005: New Berriasian palaeopole from the Central West Carpathians (Tatra Mts, southern Poland): does it look Apulian? *Geophys. J. Internat.* 161, 65–80.

Grabowski J. 2011: Magnetostratigraphy of the Jurassic/Cretaceous boundary interval in the Western Tethys and its correlations with other regions: a review. *Volumina Jurassica* 9, 105–128.

Grabowski J. & Pszczółkowski A. 2006: Magneto- and biostratigraphy of the Tithonian–Berriasian pelagic sediments in the Tatra Mountains (central Western Carpathians, Poland): sedimentary and rock magnetic changes at the Jurassic/Cretaceous boundary. *Cretaceous Res.* 27, 398–417.

Grabowski J., Michalík J., Szaniawski R. & Grotek I. 2009: Synthrusting remagnetization of the Krížna Nappe: high resolution palaeo- and rock magnetic study in the Strážovce section, Strážovske vrchy Mts, Central West Carpathians (Slovakia). *Acta Geol. Pol.* 59, 137–155.

Grabowski J., Michalík J., Pszczółkowski A. & Lintnerová O. 2010: Magneto- and isotope stratigraphy around the Jurassic/Cretaceous boundary in the Vysoká Unit (Male Karpaty Mountains): correlations and tectonic implications. *Geol. Carpath.* 61, 309–326.

Grabowski J., Schnyder J., Sobień K., Koptiková L., Krzemiński L., Pszczółkowski A., Hejnar J. & Schnabl P. 2013: Magnetic susceptibility and spectra gamma logs in the Tithonian–Berriasian pelagic carbonates in the Tatra Mts (Western Carpathians, Poland): palaeoenvironmental changes at the Jurassic/Cretaceous boundary. *Cretaceous Res.* 27, 398–417.

Grabowski J., Krzemiński L., Schnyder J., Sobień K., Hejnar J., Koptíková L., Pszczółkowski A. & Schnabl P. 2014: Integrated magnetic susceptibility and geochemical record of δ13C Anomalies in the Berriasian and Valanginian sections from the Tethyan domain (Western Carpathians, Poland). In: Rocha R. et al. (Ed.): STRATI 2013. *Springer Geology*, 847–851.

Grandesso P. 1977: On Tithoinian beds with praecalpionellids reported from Rosso Ammonitico Veneto [Gli strati a Precalpionellidi del Titoniano e I loro raporti con il Rosso Ammonitico Veneto]. *Memoire di Scienze Geologiche* 32, 1–15 (in Italian).

Gröcke D.R., Price G.D., Ruffell A.H., Mutterlose J. & Baraboshkin E. 2003: Isotopic evidence for Late Jurassic–Early Cretaceous climate change. *Palaeogeogr. Palaeoclimatol. Palaeoecol.* 202, 97–118.

Haq B.U. 2014: Cretaceous eustasy revisited. *Global and Planetary Change* 113, 44–58.

Haško J. 1978: The Orava Unit — new unit of the Klippen Belt, Western Carpathians. *Geologické práce, Správy* 70, 115–121 (in Slovak).

Houša V., Krs M., Krsová M. & Pruner P. 1996: Magnetostratigraphic and micro-paleontological investigations along the Jurassic–Cretaceous boundary strata, Brodno near Žilina (Western Slovakia). *Geol. Carpath.* 47, 3, 135–151.

Houša V., Krs M., Krsová M., Man O., Pruner P. & Venhodová D. 1999: High-resolution magnetostratigraphy and micropaleontology across the J/K boundary strata at Brodno near Žilina, western Slovakia: summary results. *Cretaceous Res.* 20, 699–717.

Houša V., Krs M., Man O., Pruner P., Venhodová D., Cecca F., Nardi G. & Piscitello M. 2004: Combined magnetostratigraphic, palaeomagnetic and calpionellid investigations across the Jurassic/Cretaceous boundary strata in the Bosso Valley, Umbria, central Italy. *Cretaceous Res.* 25, 771–785.

Houša V., Pruner P., Zakharov V.A., Košťák M., Chadima M., Rogov M.A., Šlechta S. & Mazuch M. 2007: Boreal–Tethyan correlation of the Jurassic/Cretaceous boundary interval by Palaeoenvironments and palaeoceanography changes across the J/K boundary magneto- and biostratigraphy. *Stratigraphy and Geological Correlation* 15, 297–309.

Hüneke H. & Stow D.A.V. 2008: Chapter 17: Identification of ancient contourites: Problems and paleoceanographic significance. In: Rebesco M. & Camerlenghi A. (Eds): Contourites. *Developments in Sedimentology* 60, *Elsevier*, 323–344.

Jach R., Reháková D. & Uchman A. 2012: Biostratigraphy and palaeoenvironment of the Kimmeridgian–Lower Tithonian pelagic deposits of the Krížna Nappe, Lejowa Valley, Tatra Mts. (southern Poland). *Geol. Quarterly* 56, 4, 773–788.

Lakova I. & Petrova S. 2013: Towards a standard Tithonian to Valanginian calpionellid zonation of the Tethyan Realm. *Acta Geol. Pol.* 63, 2201–221.

Lakova I., Stoykova K. & Ivanova D. 1999: Calpionellid, nannofossils and calcareous dinocyst bioevents and integrated biochronology of the Tithonian to Valanginian in the West Balkan Mountains, Bulgaria. *Geol. Carpath.* 50, 151–168.

Lowrie W. 1990: Identification of ferromagnetic minerals in a rock by coercivity and unblocking temperature properties. *Geophys. Res. Lett.* 17, 2, 159–162.

Lukeneder A., Halásová E., Kroh A., Mayrhofer S., Pruner P., Reháková D., Schnabl P., Spovieri M. & Wagreich M. 2010: High resolution stratigraphy of the Jurassic–Cretaceous boundary interval in the Gresten Klippenbelt (Austria). *Geol. Carpath.* 61,5, 365–381.

Márton E., Grabowski J., Plašienka D., Túnyi I., Krobicki M., Haas J. & Pethe M. 2013: New paleomagnetic results from the Upper Cretaceous red marls of the Pieniny Klippen Belt, Western Carpathians: evidence for general CCW rotation and implication for the origin of the structural arc formation. *Tectonophysics* 592, 1–13.

Márton E., Grabowski J., Tokarski A.K. & Túnyi I. 2015: Paleomagnetic results from the fold and thrust belt of the Western Carpathians: an overview. In: Pueyo E.L., Cifelli F., Sussman A.J. & Oliva-Urcia B. (Eds): Palaeomagnetism in fold and thrust belts: New perspectives. *Geol. Soc. London, Spec. Publ.* 425, doi:10.1144/SP425.1.

McFadden P.L. & McElhinny M.W. 1990: Classification of the reversal test in paleomagnetism. *Geophys. J. Internat.* 103, 725–729.

Melinte M. & Mutterlose J. 2001: A Valanginian (E. Cretaceous) "Boreal nannoplankton excursion" in sections from Romania. *Mar. Micropaleont.* 43, 1–25.

Michalík J. 1994: Notes on the paleogeography and paleotectonics

of the Western Carpathian area during the Mesozoic. *Mitt. Österr. Geol. Gesell.* 86, 101–110.

Michalík J. 2007: Sedimentary rock record and microfacies indicators of the latest Triassic to mid-Cretaceous tensional development of the Zliechov Basin (central Western Carpathians). *Geol. Carpath.* 58, 5, 443–453.

Michalík J. & Reháková D. 2011: Possible markers of the Jurassic/Cretaceous boundary in the Mediterranean Tethys — A review and state of art. *Geoscience Frontiers* 2, 475–490.

Michalík J., Reháková D., & Peterčáková M. 1990: To the stratigraphy of Jurassic–Cretaceous boundary beds in the Kysuca sequence of the West Carpathian Klippen belt Brodno section near Žilina. *Zemní Plyn a Nafta* 9b, 57–71.

Michalík J., Reháková D., Hladíková J. & Lintnerová O. 1995: Lithological and biological indicators of orbital changes in Tithonian and Lower Cretaceous sequence, Western Carpathians, Slovakia. *Geol. Carpath.* 46, 3, 161–174.

Michalík J., Lintnerová O., Bak M., Skupien P., Soták J., Halásová E. & Boorová D. 2008: Sedimentary, biological and isotopic record of Early Aptian paleoclimatic event in the Pieniny Klippen Belt, Slovak Western Carpathians. *Cretaceous Res.* 29, 871–892.

Michalík J., Reháková D., Halásová E. & Lintnerová O. 2009: The Brodno section — a potential regional stratotype of the Jurassic/Cretaceous boundary (Western Carpathians). *Geol. Carpath.* 60, 3, 213–232.

Ogg J.G. 2012: Geomagnetic Polarity Time Scale. In: Gradstein F.M. et al. (Eds): The Geologic Time Scale 1, 85–113.

Ogg J.G., Hasenyager R.W., Wimbledon W.A., Channell J.E.T. & Bralower T.J. 1991: Magnetostratigraphy of the Jurassic–Cretaceous boundary interval — Tethyan and English faunal realms. *Cretaceous Res.* 12, 455–482.

Ondrejíčková A., Borza V., Korábová K. & Michalík J. 1993: Calpionellid, radiolarian and calcareous nannoplankton association near the Jurassic–Cretaceous boundary (Hrušové section, Čachtické Karpaty Mts, Western Carpathians). *Geol. Carpath.* 44, 3, 177–188.

Plašienka D. 2003: Dynamics of Mesozoic pre-orogenic rifting in the Western Carpathians. *Mitt. Österr. Geol. Gesell.* 94, 79–98.

Pop G. 1974: Les zones des Calpionelles Tithonique–Valanginiens du silon de Resita (Carpates meridionales). *Revue Roumaine de Géologie Géophysique et Géographie, sér. Géol* 18, 109–125.

Price G.D., Főzy I. & Pálfy J. 2016: Carbon cycle history through the Jurassic–Cretaceous boundary: A new global $\delta^{13}C$ stack. *Palaeogeogr. Palaeoclimatol. Palaeoecol.* 451, 46–61.

Pruner P., Houša V., Oloriz F., Košťák M., Man O., Schnabl P., Venhodová D., Tavera J.M. & Mazuch M. 2010: High-resolution magnetostratigraphy and biostratigraphic zonation of the Jurassic/Cretaceous boundary strata in the Puerto Escaño section (southern Spain). *Cretaceous Res.* 31, 2, 192–206.

Reháková D. 1995: New data on calpionellid distribution in the Upper Jurassic/Lower Cretaceous formations (Western Carpathians). *Miner. Slovaca* 27, 308–318 (in Slovak).

Reháková D. 2000a: Evolution and distribution of the Late Jurassic and Early Cretaceous calcareous dinoflagellates recorded in the Western Carpathians pelagic carbonate facies. *Miner. Slovaca* 32, 79–88.

Reháková D. 2000b: Calcareous dinoflagellate and calpionellid bioevents versus sea-level fluctuations recorded in the West-Carpathian (Late Jurassic/Early Cretaceous) pelagic environments. *Geol. Carpath.* 51, 4, 229–243.

Reháková D. & Michalík J. 1994: Abundance and distribution of late Jurassic–Early Cretaceous microplankton in Western Carpathians. *Geobios* 27, 135–156.

Reháková D. & Michalík J. 1997: Evolution and distribution of calpionellids — the most characteristic constituents of Lower Cretaceous Tethyan microplankton. *Cretaceous Res.* 18, 493–504.

Reháková D., Halásová E. & Lukeneder A. 2009: The Jurassic–Cretaceous boundary in the Gresten Klippenbelt (Nutzhof, Lower Austria): Implications for micro- and nannofacies analysis. *Ann. Naturhist. Mus. Wien* 110 A, 345–381.

Reháková D., Matyja B.A., Wierzbowski A., Schlögl J., Krobicki M. & Barski M. 2011: Stratigraphy and microfacies of the Jurassic and lowermost Cretaceous of the Veliky Kamenets section (Pieniny Klippen Belt, Carpathians, Western Ukraine). *Volumina Jurassica* 9, 61–104.

Remane J., Borza K., Nagy I., Bakalova-Ivanova D., Knauer J., Pop G. & Tardi-Filácz E. 1986: Agreement on the subdivision of the standard calpionellid zones defined at the IInd Planktonic Conference Roma 1970. *Acta Geol. Hung.* 29, 5–14.

Satolli S., Turtu A., & Donatelli U. 2015. Magnetostratigraphy of the Salto del Cieco section (Northern Appenines, Italy) from the Pliensbachian to Jurassic/Cretaceous boundary. *Newsletters on Stratigraphy* 48, 2, 153–177.

Schlögl J., Aubrecht R. & Tomašových A. 2000: The first find of the Orava Unit in the Púchov section of the Pieniny Klippen Belt (western Slovakia). *Miner. Slovaca* 32, 45–54.

Schnabl P., Pruner P. & Wimbledon W.A.P. 2015: A review of magnetostratigraphic results from the Tithonian–Berriasian of Nordvik (Siberia) and possible biostratigraphic constraints. *Geol. Carpath.* 66, 6, 489–498.

Shurygin B.N., Dzyuba O.S., Izokh O.P., Kosenko L.N. & Kuznetsov A.B. 2015: Isotope markers (C, O, Sr) of the Jurassic–Cretaceous Boundary beds in Boreal regions (Maurynya section, Western Siberia). In: Zakharov V.A., Rogov M.A. & Ippolytov A.P. (Eds.): Jurskaya Sistema Rossii. *VI. All-Russian Symposium*, Makhachkala, 318–320.

Street C. & Bown P.R. 2000: Palaeobiogeography of early Cretaceous (Berriasian–Barremian) calcareous nannoplankton. *Mar. Micropaleont.* 39, 265–291.

Svobodová A. & Košťák M. 2016: Calcareous nannofossils of the Jurassic–Cretaceous boundary strata in the Puerto Escaño section (southern Spain) — biostratigraphy and palaeoecology. *Geol. Carpath.* 67, 3, 223–238.

Švábenická L. 2012: Nannofossil record across the Cenomanian–Coniacian interval in the Bohemian Cretaceous Basin and Tethyan foreland basins (Outer Western Carpathians), Czech Republic. *Geol. Carpath.* 63, 3, 201–217.

Tappan H. 1993: Tintinnids. In: Lipps J.H. (Ed.): Fossil Prokaryotes and Protists. *Blackwell*, Oxford, 285–303.

Tremolada F., Bornemann A., Bralower T.J., Koeberl C. & van de Schootbrugge B. 2006: Paleoceanographic changes across the Jurassic/Cretaceous boundary: the phytoplankton response. *Earth Planet. Sci. Lett.* 241, 361–371.

Van der Voo R. 1993: Paleomagnetism of the Atlantic, Tethys and Iapetus Oceans. *Cambridge University Press*, 1–411.

Vandenbroucke T.R.A., Emsbo P., Munnecke A., Nuns N., Duponchei L., Lepot K., Quijada M., Paris F., Servais T. & Kiessling W. 2015: Metal-induced malformations in Early Palaeozoic plankton are harbingers of mass extinction. *Nature Communications* 6, doi:10.1038/ncomms8966.

Weissert H. & Channell J.E.T. 1989: Tethyan carbonate C isotope stratigraphy across the Jurassic–Cretaceous boundary: An indicator of decoelerated carbon cycling. *Paleoceanography* 4, 483–494.

Weissert H. & Lini A. 1991: Ice age interludes during the time of Cretaceous greenhouse climate? In: Müller D.W., McKenzie J.A. & Weissert H. (Eds.): Controversies in modern geology. *Acad. Press*, London, 173–191.

Weissert H. & Mohr H. 1996: Late Jurassic climate and its impact on carbon cycling. *Palaeogeogr. Palaeoclimatol. Palaeoecol.* 122, 27–43.

Wimbledon W.A.P., Reháková D., Pszczółkowski A. Casellato C.E.,

Halásová E., Frau C., Bulot L.G., Grabowski J., Sobień K., Pruner P., Schnabl P. & Čížková K. 2013: An account of the bio- and magnetostratigraphy of the upper Tithonian–lower Berriasian interval at Le Chouet, Drôme (SE France). *Geol. Carpath.* 64, 6, 437–400.

Zakharov V.A., Rogov M.A., Dzyuba O.S., Žák K., Košťák M., Pruner P., Skupien P., Chadima M., Mazuch M. & Nikitenko B.L. 2014: Palaeoenvironments and palaeoceanography changes across the Jurassic/Cretaceous boundary in the Arctic realm: case study of the Nordvik section (north Siberia, Russia). *Polar Research* 33, 19714, doi:10.3402/polar.v33.19714

Žák K., Košťák M., Man O., Zakharov V.A., Rogov M.A., Pruner P., Rohovec J., Dzyuba O.S. & Mazuch M. 2011: Comparison of carbonate C and O stable isotope records across the Jurassic/Cretaceous boundary in the Tethyan and Boreal Realms. *Palaeogeogr. Palaeoclimatol. Palaeoecol.* 299, 83–96.

Appendix: List of microfossils

Calpionellids

Longicollaria dobeni (Borza, 1966)
Carpathella rumanica Pop, 1998
Borziella slovenica (Borza, 1969)
Dobeniella tithonica (Borza, 1969)
Chitinoidella boneti Doben, 1963
Dobeniella cubensis (Furrazola-Bermúdez, 1965)
Popiella oblongata Reháková, 2002
Praetintinnopsella andrusovi Borza, 1969
Crassicollaria intermedia (Durand Delga, 1957)
Crassicollaria massutiniana (Colom, 1948)
Crassicollaria brevis Remane, 1962
Crassicollaria parvula Remane, 1962
Crassicollaria colomi Doben, 1963
Calpionella alpina Lorenz, 1902
Calpionella grandalpina Nagy, 1986
Calpionella elliptalpina Nagy,1986
Calpionella elliptica Cadisch, 1932
Calpionella minuta Houša,1990
Tintinnopsella carpathica (Murgeanu and Filipescu, 1933)
Tintinopsella doliphormis (Colom, 1939)
Tintinnopsella longa (Colom, 1939)
Tintinnopsella remanei Borza1969
Remaniella ferasini (Catalano, 1965)
Remaniella catalanoi Pop, 1996
Remaniella duranddelgai Pop, 1996
Remaniella colomi Pop, 1996
Remaniella borzai Pop, 1996
Remaniella filipescui Pop, 1996
Remaniella cadischiana Pop, 1996
Lorenziella hungarica Knauer and Nagy,1964
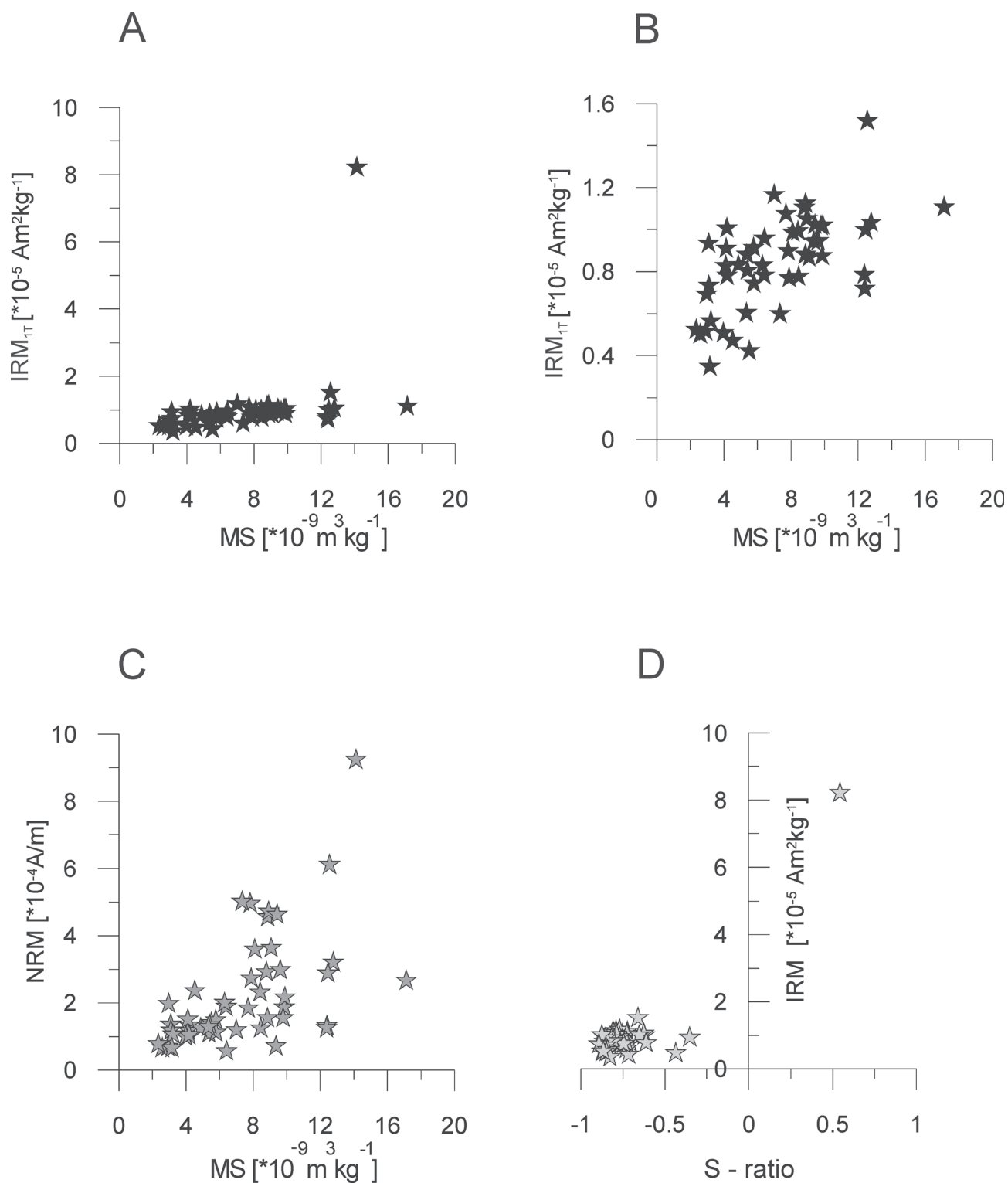
Calcareous dinoglagellates

Stomiosphaera moluccana Wanner, 1940
Carpistomiosphaera borzai (Nagy, 1966)
Colomisphaera nagyi (Nagy, 1966)
Colomisphaera pulla (Borza, 1964)
Colomisphaera radiata (Vogler, 1941)
Colomisphaera tenuis (Nagy, 1966)
Colomisphaera fortis Řehánek, 1992
Colomisphaera lapidosa (Colom, 1935)
Colomisphaera carpathica (Borza, 1964)
Parastomiosphaera malmica (Borza, 1964)
Stomiosphaerina proxima Řehánek, 1987
Cadosina semiradiata fusca (Wanner,1940)
Cadosina semiradiata semiradiata (Wanner,1940)

Another microfossils

Gemeridella minuta Borza et Mišík 1975
Didemnoides moreti Durand-Delga
Didemnum carpaticum Borza et Mišík 1975
Globochaeta alpina Lombard 1945.

Calcareous nannofossils

Assipetra infracretacea (Thierstein, 1973) Roth, 1973
Conusphaera mexicana (Trejo, 1969) subsp. *mexicana* Bralower in Bralower et al. 1989
Conusphaera mexicana (Trejo, 1969) subsp. *minor* (Bown et Cooper, 1989), Bralower in Bralower et al. 1989
Cyclagelosphaera deflandrei (Manivit, 1966) Roth, 1973
Cyclagelosphaera margerelii Noël, 1965
Diazomatolithus lehmanii Noël, 1965
Faviconus multicolumnatus Bralower in Bralower et al. 1989
Hexalithus noeliae (Noël, 1956) Loeblich et Tappan, 1966
Lithraphidites carniolensis Deflandre, 1963
Microstaurus chiastius (Worsley, 1971) Bralower et al., 1989
Nannoconus sp. Kamptner, 1931
Nannoconus erbae Casellato, 2010
Nannoconus globulus (Brönnimann, 1955) subsp. *globulus* Bralower in Bralower et al. 1989
Nannoconus globulus (Brönnimann, 1955) subsp. *minor* Bralower in Bralower et al. 1989
Nannoconus infans Bralower in Bralower et al. 1989
Nannoconus kamptneri (Brönnimann, 1955) subsp. *minor* Bralower in Bralower et al. 1989
Nannoconus steinmannii (Kamptner, 1931) subsp. *minor* Deres et Achérítéguy, 1980
Nannoconus steinmannii (Kamptner, 1931) subsp. *steinmannii* Deres et Achérítéguy, 1980
Nannoconus wintereri Bralower et Thierstein in Bralower et al. 1989
Polycostella beckmannii Thierstein, 1971
Retacapsa sp. Black, 1971
Watznaueria barnesiae (Black in Black et Barnes, 1959) Perch-Nielsen, 1968
Watznaueria biporta Bukry, 1969
Watznaueria britannica (Stradner, 1963) Reinhardt, 1964
Watznaureia fossacincta (Black, 1971a) Bown in Bown et Cooper 1989
Watznaueria manivitiae (Bukry, 1973) Moshkovitz et Ehrlich, 1987
Watznaueria ovata Bukry, 1969
Zeugrhabdotus embergeri (Noël, 1958) Perch-Nielsen, 1984
Zeugrhabdotus erectus (Deflandre in Deflandre et Fert, 1954) Reinhardt, 1965

Supplementum

Supplementary Fig. S1. NRM intensity, MS, IRM$_{1T}$ and S-ratio in the Strapkova section, against biostratigraphy and magnetostratigraphy. Details of magnetostratigraphic interpretations are presented in the Fig. 15.

Supplementary Fig. S2. Rock magnetic correlations in Strapkova sections. **A** — MS vs. IRM$_{1T}$; **B** — MS vs. IRM$_{1T}$ without anomalous sample 296.5; **C** — MS vs. NRM; **D** — S-ratio vs. IRM$_{1T}$.
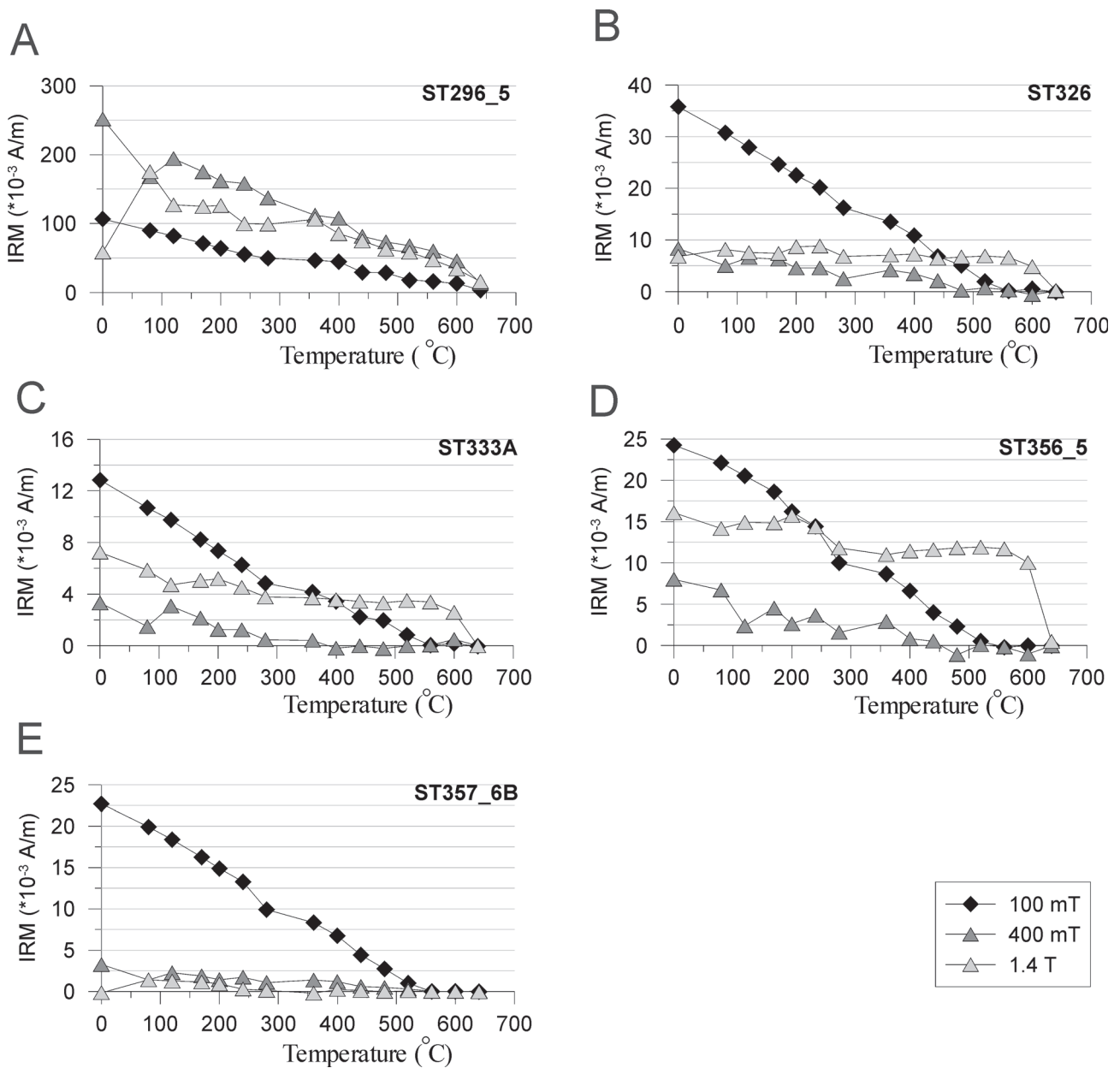
Supplementary Fig. S3. Thermal demagnetization of the IRM acquired in the fields of 0.1T, 0.4T and 1T in three perpendicular directions:

A — sample 296.5, Late Tithonian Crassicollaria colomi Subzone, M19n2n magnetozone (S-ratio=0.54)

B — sample 326, Early Berriasian Calpionella alpina Subzone, M19n2n magnetozone (S-ratio=−0.63)

C — sample 333, Early Berriasian Calpionella alpina Subzone, M18r magnetozone (S-ratio=−0.63)

D — sample 356.5, Early Berriasian Calpionella elliptica Subzone, M17r magnetozone, (S-ratio=−0.35)

E — sample 357.6, Early Berriasian Calpionella elliptica Subzone, M17r magnetozone, (S-ratio=−0.85)